Modeling investigation of light absorbing aerosols in the central Amazon during the wet season

Qiaoqiao Wang[1], Jorge Saturno[1], Xuguang Chi[1,a], David Walter[1], Jost V. Lavric[2,3], Daniel Moran- Zuloaga[1], Florian Ditas[1], Christopher Pöhlker[1], Joel Brito[4,b], Samara Carbone[4,c], Paulo Artaxo[4], and Meinrat O. Andreae[1]

[1]Biogeochemistry Department, Max Planck Institute for Chemistry, 55131 Mainz, Germany
[2]Department of Biogeochemical Systems, Max Planck Institute for Biogeochemistry, 07745 Jena, Germany
[3]ICOS ERIC Head Office, Helsinki, Finland
[4]Department of Applied Physics, University of São Paulo, São Paulo 05508, Brazil
[a]Now at School of Atmospheric Sciences, Nanjing University, Jiangsu, China
[b]Now at Laboratory for Meteorological Physics, University Blaise Pascal, Aubière, France
[c]Now at Federal University of Uberlândia

Correspondence to: Qiaoqiao Wang (q.wang@mpic.de)

Abstract. We use a global chemical transport model (GEOS-Chem) to interpret observed light absorbing aerosols in Amazonia during the wet season. Observed aerosol properties, including black carbon (BC) concentration and light absorption, at the Amazon Tall Tower Observatory (ATTO) site in the central Amazon have relatively low background levels, but frequently show high peaks during the study period of Jan-Apr 2014. With daily temporal resolution for open fire emissions and modified aerosol optical properties, our model successfully captures the observed variation of fine/coarse aerosol and BC concentrations as well as aerosol light absorption and its wavelength dependence over the Amazon basin. The source attribution in the model indicates the important influence of open fire on the observed variances of aerosol concentrations and absorption, mainly from regional sources (northern South America) and from Northern Africa. The contribution of open fires from these two regions are comparable, with the latter becoming more important in the late wet season. The analysis of correlation and enhancement ratios of BC versus CO suggests transport times of < 3 d for regional fires and ~ 11 d for African plumes arriving at ATTO during the wet season. The model performance of long-range transport of African plumes is also evaluated with observations from AERONET, MODIS, and CALIOP. Simulated absorption aerosol optical depth (AAOD) averaged over the wet season is lower than 0.002 in most of the Amazon region, including the ATTO site. We find that more than 50 % of total absorption at 550 nm is from BC, except for the northeastern Amazon and the Guyanas, where the influence of dust becomes significant (up to 35 %). The brown carbon contribution is generally between 20-30 %. The distribution of absorption Ångström exponents (AAE) suggests more influence from fossil fuel combustion in the southern part (AAE ~ 1), but more open fire and dust influence in the northern part of the basin (AAE > 1.8). Uncertainty analysis shows that accounting for absorption due to secondary organic aerosol (SOA) and primary biogenic aerosol (PBA) particles could result in differences of < 8 % and 5-40 % in total absorption, respectively.

1 Introduction

Light-absorbing aerosols (LAA) are of climatic interest as strong absorber of solar radiation in the atmosphere. They alter the radiative balance of the atmosphere through a complex web of processes, leading to a positive top-of-atmosphere forcing, heating of the atmosphere, and surface dimming (Ramanathan and Carmichael, 2008). Light absorption in the atmosphere is dominated by black carbon (BC), emitted from combustion sources, with a smaller contribution from mineral dust (Bond et al., 2013; IPCC, 2013; Jacobson, 2001; Ramanathan and Carmichael, 2008). Recent work has shown that light absorbing organic aerosols, known as brown carbon (BrC), may also be important, contributing 20-40 % of total carbonaceous aerosol absorption globally (Andreae and Gelencsér, 2006; Bahadur et al., 2012; Chung et al., 2012a; Chung et al., 2012b; Lin et al., 2014; Saleh et al., 2015). However, the poor knowledge of the LAA's atmospheric concentrations and optical properties leads to large uncertainties in estimating the absorption attributable to LAA species, and consequently in estimating the radiative forcing of total aerosols (Andreae and Ramanathan, 2013; Bond et al., 2013; Kim et al., 2014; Kinne et al., 2006; Myhre et al., 2013; Saleh et al., 2015; Schulz et al., 2006; Sinyuk et al., 2003; Wang et al., 2014a).

The Amazon basin, being the world's largest rainforest area, plays an important role in Earth's climate system. Scientific concern has been shifting from regional climate change over the Amazon basin to the interactions of global climate change with the functioning of the Amazon basin' ecosystem (Andreae et al., 2015). Therefore, understanding sources, concentrations, and properties of aerosols in the Amazon basin is important from both regional and global points of view. During the wet season (January-April), the Amazon basin is in near-pristine conditions, and therefore this unique environment provides a baseline understanding against which to assess anthropogenic effects (Andreae, 2007; Martin et al., 2010a).

Over the past decades, numerous field campaigns with measurements of aerosols and their optical properties have been carried out in the Amazon basin. A summary of sources and properties of Amazonian aerosols can be found in the reviews of Martin et al. (2010a; 2010b) and Andreae et al. (2015). Briefly, Amazonian aerosols are dominated by local and regional biogenic aerosols in the wet season, with remarkably low concentrations (a few $\mu g\ m^{-3}$) and absorption coefficients (~0.5 Mm^{-1} at wavelength of 550 nm) (Guyon et al., 2003a; Guyon et al., 2003b; Rizzo et al., 2013; Rizzo et al., 2011). The near-pristine conditions are episodically interrupted by long-range transport of Saharan dust and African biomass burning and fossil fuel combustion aerosols, which significantly elevate the absorption coefficients (Andreae et al., 2015; Baars et al., 2011; Ben-Ami et al., 2010; Formenti et al., 2001; Guyon et al., 2003b; Martin et al., 2010a; Martin et al., 2010b; Rizzo et al., 2013). While species other than BC, such as biogenic aerosols, are suggested to be responsible for a substantial fraction to the total absorption (Guyon et al., 2003b, 2004; Rizzo et al., 2010), the contribution of the different species to total observed aerosol absorption is not clear yet.

Attempts to model Amazonian aerosols are limited, with focus either on dust deposition (e.g., Ridley et al., 2012; Yu et al., 2015) or biomass burning aerosols in the dry season (e.g., Castro Videla et al., 2013; Martins and Pereira, 2006; Rosário et al., 2013). Here we present a detailed simulation of LAA in the Amazon basin in the wet season with the GEOS-Chem CTM. We show that the GEOS-Chem model successfully captures the observed variation and magnitude of LAA mass con-

centration as well as the associated absorption and its wavelength dependence. In addition to long-range transport of African dust and open fire aerosols, we show that regional open fires are also responsible for observed enhancement of aerosol mass and absorption in wet season.

2. Model Description

5 We use the GEOS-Chem CTM version 9-02 (http://www.geos-chem.org/) driven by assimilated meteorological data GEOS-FP from NASA Global Modeling and Assimilation Office (GMAO). The GEOS-FP data have 1-hourly and 3-hourly temporal resolution, 47 vertical layers, and $0.25° \sim 0.3125°$ horizontal resolution. We degrade the horizontal resolution to $2° \sim 2.5°$ for input to GEOS-Chem. We initialize the model with a 6-month spin-up followed by simulation of Jan-Apr 2014.

Aerosol types simulated in GEOS-Chem include carbonaceous aerosols, sulfate-nitrate-ammonium aerosols, sea salts, and
10 mineral dust. The simulation of carbonaceous aerosols was originally described by Park et al. (2003). Black carbon and primary organic aerosol (POA) are emitted by fuel (fossil fuel and biofuel) combustion and open fires. Note that "black carbon" used here implies particles having optical properties and composition similar to "soot carbon" as defined by Andreae and Gelencsér (2006). We assume that 80 % of BC and 50 % of POA are emitted as hydrophobic particles and convert them to hydrophilic in the atmosphere with an e-folding time of 1 day, which yields a good simulation of BC export efficiency in
15 continental outflow (Park et al., 2005). To account for the non-carbon mass in POA, we apply a factor of 1.7 to the simulated organic carbon (OC) mass concentration, to be consistent with the measurements in the Amazon Basin (Chen et al., 2015; Chen et al., 2009). The simulation of BC and POA in GEOS-Chem are linear, with concentrations proportional to sources. We isolate the contributions from different sources by tagging them in the model. Secondary organic aerosol (SOA) is produced in the atmosphere as oxidation products of biogenic (monoterpenes, sesquiterpenes, and isoprene) and aromatic pre-
20 cursors (Chung and Seinfeld, 2002; Henze and Seinfeld, 2006; Henze et al., 2008; Pye et al., 2010). Note that the simulation of carbonaceous aerosol does not include primary biogenic aerosol (PBA), which likely dominates the coarse aerosols in the Amazon (Pöschl et al., 2010). We discuss the uncertainties associated with PBA particles later in this paper.

The simulation of mineral dust was described in detail by Fairlie et al. (2007). Briefly, the model uses the dust entrainment and deposition (DEAD) mobilization scheme of Zender et al. (2003) for calculation of sources and emission. Dust par-
25 ticles are emitted in four size bins (radii 0.1-1.0, 1.0-1.8, 1.8-3.0 and 3.0-6.0 μm), with corresponding mass fractions of 12.2 %, 25.3 %, 32.3 % and 30.2 %. The smallest size bin is further divided into four sub-bins (radii 0.1-0.18, 0.18-0.3, 0.3-0.6 and 0.6-1.0 μm) for optical properties, which are strongly size dependent for sub-micron aerosols. The mass fraction in each bin is 6 %, 12 %, 24 % and 58 % from smallest to largest, constrained from aircraft PCASP measurements of Saharan dust (Ridley et al., 2012).

30 Dry deposition in GEOS-Chem follows a standard resistance-in-series scheme (Wesely, 1989) as implemented by Wang et al. (1998), accounting for gravitational settling and turbulent dry transfer of particles to the surface (Zhang et al., 2001). Wet deposition in GEOS-Chem was initially based on the scheme of Liu et al. (2001), which includes scavenging in convective updrafts, as well as in-cloud and below-cloud scavenging from convective and large-scale precipitation. We adopt the

update of the scheme by Wang et al. (2011; 2014a), which accounts for scavenging by cold (ice) clouds and snow as well as the impaction scavenging during convective updrafts.

Aerosol optical depth (AOD) and absorption aerosol optical depth (AAOD) is calculated online assuming log-normal size distributions of externally mixed aerosols and accounting for hygroscopic growth (Martin et al., 2003). Aerosol optical prop-
5   erties used in the calculation are based on the Global Aerosol Data Set (GADS) data (Koepke et al., 1997), with modification in size distribution (Drury et al., 2010; Jaeglé et al., 2011; Wang et al., 2003a; Wang et al., 2003b), hygroscopic growth factors, and the refractive index of dust (Sinyuk et al., 2003).

2.1. Treatment of black carbon and brown carbon

Table 1 lists the optical properties used in GEOS-Chem for LAA at a wavelength of 550 nm and dry conditions. The stand-
10   ard GEOS-Chem does not account for the absorption enhancement due to the mixing state of BC and thus has a low value of 5.9 m^2 g^{-1} for BC mass absorption efficiency (MAE) at 550 nm. Previous studies have shown that BC MAE could be enhanced by a factor up to two with values in the range of 9-12 m^2 g^{-1} (Bond and Bergstrom, 2006; Bond et al., 2013). In this work, we scale the MAE at 550 nm to 12 m^2 g^{-1} assuming thick coating due to the abundance of SOA in the Amazon basin (Chen et al., 2009; Pöschl et al., 2010). We also update the absorption Ångström exponents (AAE) for BC from 1.3 to 0.5
15   based on the study by Chung et al. (2012b) and Bahadur et al. (2012), assuming that this lowest observed value represents BC, without too much contamination by brown carbon or dust.

In addition to the update in BC properties, we add the contribution of brown carbon (BrC) in the model. Brown carbon absorbs solar radiation, particularly at UV wavelengths, and thus its absorption spectrum shows a strong wavelength dependence. The standard GEOS-Chem, however, does not separate BrC from "white" carbon (non-absorbing carbon), but assumes
20   slight absorption for all kinds of OA and weak wavelength dependence with AAE of 0.8 between wavelength of 550 and 400 nm. In this work, we assume that all POA from biofuel and open fires is BrC. The refractive index is based on the work of Saleh et al. (2015), who parameterized the absorptivity of BrC as a function of emission ratio of BC versus OA. The derived imaginary part of the refractive index and the AAE at 550 nm are 0.023 and 2.5 m^2 g^{-1} for biofuel OA and 0.017 and 3.1 m^2 g^{-1} for open fire OA.

25   The refractive index of dust at 550 nm in GEOS-Chem is 1.56-0.0014i, yielding an MAE from 0.017 m^2 g^{-1} to 0.028 m^2 g^{-1} depending on the size distribution. The MAE for total dust aerosol increases as it is transported away from the source regions, because coarse aerosols are more susceptible to deposition.

2.2. Emissions of carbonaceous aerosols

Table 2 gives regional and global totals for BC and organic aerosol (OA) during Jan-Apr 2014 in GEOS-Chem and Fig. 1
30   shows the distribution of BC and OA emissions over 120 °W–60 °E during the same period. We tagged BC and POA tracers from either fuel combustion or open fire from seven regions as defined in Table 2: NA (North America), CA (Central America), NSA (Northern South America), SSA (Southern South America), Europe, NAF (Northern Africa) and SAF (Southern

Africa). Note that NSA includes the Amazon Basin as well as large portion of Brazil. We use the region NSA to represent the Amazon basin. The emissions of BC and POA are from Bond et al. (2007) for fuel combustion and from Fire Inventory from NCAR version 1.5 (FINNv1.5) (Wiedinmyer et al., 2011) with daily resolution for open fire. Emissions of SOA pre-cursors are from MEGAN (Model of Emissions of Gases and Aerosols from Nature) v2.1 (Guenther et al., 2006) for biogen-
5 ic VOC and from RETRO (REanalysis of the TROpospheric chemical composition) (Schultz et al., 2007) for aromatics.

Global total emissions of BC are 7.2 Tg a^{-1}, 37 % of which are from open fire. NAF has the highest BC emission (0.93 Tg a^{-1}) and open fire contribution (66 %) among all defined seven regions. In contrast, emissions of BC over NSA are quite small (0.23 Tg a^{-1}), 20 % of which are from open fire. Total emissions of OA are about 82 Tg a^{-1} (61 Tg a^{-1} for POA and 22 Tg a^{-1} for SOA). The distribution of POA emissions is similar to that of BC, but with more open fire contribution (74 % of
10 POA on global average). NAF again has the highest POA emissions (12 Tg a^{-1}) and open fire contribution (88 % of POA) among all 7 regions. NAF also has the highest SOA emissions of 6.4 Tg a^{-1}, which contribute 34 % of total OA emissions over the region. Total OA emissions over NSA are 5.4 Tg a^{-1}, with SOA being the largest source (accounting for 75 % of total), followed by open fires (13 %). As expected from its location and land cover, SOA in NSA are mainly biogenic.

2.3. Emissions of mineral dust

15 Figure 2 shows the distribution of dust emissions during Jan-Apr 2014 over 120 ° W–60 ° E and 60 ° S–60 ° N in GEOS-Chem. The model has a global emission of 1.2 Pg a^{-1}, 78 % of which is located in NAF as it contains most of the Sahara. There is also a small dust emission (4 % of total) in Argentina in SSA. The emissions are highly variable from month to month. In NAF, the emission in February is 30 % higher than the seasonal average, followed by the emission in March, 10 % higher than the average.

20 Due to a reduction in surface winds in the dust source regions in Africa, there is a significant downward trend from 1982 to 2008 in dustiness over the east mid-Atlantic (Ridley et al., 2014). Here we assess the model performance with regard to the dust loading over Africa during the study period of Jan-Apr 2014 by Aerosol Robotic Network (AERONET) surface observations and Moderate-Resolution Imaging Spectroradiometer (MODIS) data.

Figure 3 shows the time series of simulated and observed AOD at 550 nm at four AERONET sites situated at the southern
25 border of the Sahel region (see purple dots in Fig. 2). The observations are from AERONET level 2.0 daily data during Jan-Apr 2014. We find six sites with valid data covering more than 30 % of the time period. To exclude the influence of sea salt, we only use those four where dust dominates the AOD from coarse aerosol (particles with diameter > 1 μm) in the model. The observed AOD at the four sites ranges widely from 0.04 to 2.0. The model successfully captures the variation of ob-served AOD at each site, with correlation coefficients r of 0.64 – 0.81. We also diagnose for each site the normalized mean
30 bias, $NMB = \sum(M_i - O_i)/\sum O_i$, where sums are over the entire period and M_i and O_i are the simulated and observed val-ues. The model slightly overestimates the observed AOD at most sites with NMB from 5 – 21 %, except the Ilorin site, with NMB of -8 %.

Figure 4 shows the spatial distribution of simulated and MODIS AOD averaged over Jan-Apr 2014 over both Africa and the ocean. In this study we use MODIS level 3 data (daily gridded 1 °x 1 °product) from both Terra and Aqua satellites and degrid the data over the model grid. Over bright surfaces, where no successful standard retrieval is available, we use the deep blue retrieval.

Over Africa, MODIS shows strong sources in the Bodélé region, with obvious influence over its outflow regions. The model captures well the spatial distribution over the dusty region (17.5 °W–40 °E and 13 °N–35 °N, shown in Fig.4) with r of 0.76, but tends to overestimate observed AOD with NMB of 13 %. The distribution of the bias has a median of 13 % with a 25th percentile of -5.8 % and a 75th percentile of 31 %. The major underestimation in the model is over the Bodélé region, but the bias gradually becomes positive over its related outflow. The difference between the model and MODIS data is not due to sampling bias, as the results are similar when the model is sampled to only use days and locations when MODIS is available. Ridley et al. (2012) suggested that the underestimate over the Bodélé region in GEOS-Chem is due to insufficiently high resolution to represent the high wind speeds encountered between the mountain ranges in this relatively small region.

The comparison with both AERONET and MODIS shows generally slight overestimate in the model AOD over dusty regions. Because AOD is a product of dust loading and its mass extinction efficiency (MEE), the bias could be due to either or both of these factors. While dust loading over source regions is mainly driven by emissions, MEE is related to dust optical properties. To evaluate the optical properties assumed in the model, we also estimate dust MEE using long-term data of size distributions and refractive indices for African dust from AERONET sites (purple dots and triangles in Fig. 2) as input for Mie calculations. For this calculation, we use level 2.0 daily data from January to April for years 2005 to 2014. In addition, we only use data strongly influenced by dust with coarse aerosols accounting for more than 90 % of total aerosol volume so that the refractive index is representative of dust aerosols.

We obtain a refractive index of 1.47 ($\pm$0.027)-0.0033i ($\pm$0 .0021i) and MEE of 0.51$\pm$0.045 m^2 g^{-1} at 550 nm applying the same density (2.6 g cm^{-3}) as used in the model. Numbers in the brackets are variation from all sites. By comparison, the refractive index at 550 nm used in the model is 1.56-0.0014i. Our value for the real part is 6 % higher than the retrieved data, but is consistent with the range of 1.51-1.56 in the literature (McConnell et al., 2010). Consequently, the model dust MEE (0.60$\pm$0.026 m^2 g^{-1}) averaged over the dusty region is 18 % higher than AERONET-derived value. This suggests that the model positive bias in AOD is probably driven by the difference in the optical properties. In contrast to the real part, the imaginary part of the refractive index of AERONET sites shows a large variation, which yields a wide range of dust mass absorption efficiency (MAE) of 0.038$\pm$0.016 m^2 g^{-1}. The imaginary part of the refractive index and the MAE (0.021 m^2 g^{-1}) over the dusty region in the model is at the lower end of the range of AERONET sites.

3. Measurements at the ATTO site

The Amazon Tall Tower Observatory (ATTO) site is located 150 km northeast of Manaus, Brazil (59 °0.335 ´W, 2 °8.752 ´S, asterisk in Fig. 1). The site was chosen to have as little human perturbation as possible. It provides continuous observations of trace gases and aerosol properties from two 80 m towers initiated in 2012 (Andreae et al., 2015). The regionally repre-

sentative measurements can provide important constraints on sources, sinks, and optical properties of aerosols in the Amazon basin.

Measurements related to LAA at the ATTO site used in this paper include aerosol concentrations, carbon monoxide (CO) concentrations, and aerosol light absorption. The measurements are generally for air sampled at 60 m above ground, unless noted otherwise. Aerosol concentrations are from a Scanning Mobility Particle Sizer (SMPS) for fine particles ($dp \leq 1$ μm) and from an Optical Particle Sizer (OPS) for coarse aerosols ($dp > 1$ μm). We convert the measured number concentrations to mass concentrations assuming spherical particles with a density of 1.5 g cm^{-3} (Pöschl et al., 2010). The SMPS has a size range of 10–430 nm. We extrapolate the range to 1 μm by fitting the data to a Gaussian distribution, which yields a scale factor of 1.03 on average. There is also a Single Particle Soot Photometer (SP2) measuring refractory black carbon (rBC) in the size range of 70–280 nm since late February 2104. The results are scaled up by 39 % to cover the range of 70–470 nm. Dry air mole ratios of CO are from a CRDS instrument (Picarro G1302) measuring air sampled at five levels: 79, 53, 38, 24, and 4 m a.g.l.. The measurement setup is in essence a copy of the system described in Winderlich et al. (2010). As the inlets for the aerosol instruments are at 60 m a.g.l., we use in this study CO dry air mole ratios averaged between 79 and 53 m a.g.l..

Aerosol light attenuation is measured by a 7-wavelength Aethalometer (λ=370, 470, 520, 590, 660, 880, and 950 nm) at dry condition (RH < 40 %). In order to obtain absorption coefficients from Aethalometer attenuation measurements, we apply to our data the correction algorithm from Schmid et al. (2006). We also use the Multi-angle Absorption Photometer (MAAP) measurements at 637 nm as a reference, since this instrument accounts for multiple scattering effects. The impact of the filter loading effect on the correction calculations is usually negligible due to the low light-absorbing aerosol concentrations at the ATTO site. For the comparison, we interpolated the absorption at λ of 400 and 550 nm based on AAE calculated through a linear fit of multiple wavelength absorption. For further information on the measurements at the ATTO site, the reader is referred to Andreae et al. (2015).

4. Trans-Atlantic transport

Several studies have shown trans-Atlantic transport of African mineral dust to the Amazon during the wet season (Abouchami et al., 2013; Baars et al., 2011; Ben-Ami et al., 2010; Formenti et al., 2001; Kumar et al., 2014; Swap et al., 2011; Talbot et al., 1990). Here we use satellite observations to test the model's ability to capture this feature. The pattern of outflow over the ocean is obvious in Fig. 4, with elevated AOD between 0 °–15 °N in both MODIS and model data. The model captures well the spatial variation of AOD over the ocean with r of 0.96. There is no significant bias between model and MODIS data, with NMB of 0.35 %. The distribution of bias shows a median of -6.4 %, with a 25th percentile of -23 % and a 75th percentile of 16 %.

Figure 5 shows the seasonal AOD along a transect from 20 °W to 60 °W averaged over 5 °S–25 °N and Jan-Apr 2014. Both MODIS and model show a declining trend from the west of Africa towards the east of South America. However, the AOD decline is faster in the model than in MODIS, especially when approaching South America. Therefore, negative model bias is generally found in the West Atlantic Ocean. One factor contributing to this difference is the relatively low back-

ground AOD in the model (0.047) compared to MODIS (0.088). This low background might imply an underestimation of sea salt in the model.

The bias could also mean that there is too much removal in the model. Ridley et al. (2012) estimated the lifetime of dust based on the gradient of the logarithm of the AOD against time assuming first order removal of aerosol and no significant

5   change in aerosol size distribution and scattering efficiency across the Atlantic. We apply the same method and find a lifetime of 3.2 d in the model, a 14 % underestimate relative to MODIS (3.7 d). This comparison is better than the results in Ridley et al. (2012), who shows an underestimate of 25-50 % in GEOS-Chem. The better performance here may be due to different sets of meteorological fields and/or updates in wet scavenging by Wang et al. (2011).

If we separate the transect trend into two parts, 20 °W to 50 °W (ocean) and 50 °W to 60 °W (ocean-land transition), we

10   find a similar lifetime of dust over ocean between model (4.2 d) and MODIS (4.3 d), but an underestimate of 19 % in the model (1.7 d) compared with MODIS (2.1 d) over the transitional zone. The retrieval method for MODIS is different between land and ocean, which results in discontinuities in AOD observed in the coastal region with higher AOD over the land than the ocean (Levy et al., 2005). Such discontinuities could result in slower decrease in averaged AOD from 50 °W to 60 °W and thus contribute to the relatively longer lifetime compared to the model results. It is also possible that the model over-

15   estimates the removal over the transitional zone.

Figure 6 shows the daily distribution of latitudinally-averaged AOD over the region between 60 °W–20 °E and 5 °S–25 °N from MODIS and the model. Observations from MODIS show about five events of trans-Atlantic transport of aerosol plumes from Africa to South America. The most obvious plume originated on 1 March from the east of the Atlantic (20 °W) and arrived at the west of the Atlantic (50 °W) around 3-4 March. We find that the model is able to reproduce the outflow

20   events across the Atlantic Ocean with an r of 0.81.

The lifetime of aerosols along the transport path does not only depend on precipitation intensity, but also on the aerosols' vertical position. Aerosols aloft at higher altitude tend to be transported farther. Figure 7 shows curtain plots of observed and simulated extinction from 60 °W to 20 °E averaged over 5 °–10 °N and the period Jan-Apr 2014. The observation is from Cloud-Aerosol Lidar With Orthogonal Polarization (CALIOP), which provides vertical profiles of aerosol extinction at 532

25   nm in addition to total column AOD during both day and night (Young and Vaughan, 2009). We use CALIOP level 2, version 3.01, lidar data of aerosol profiles at a resolution of 5 km along the track. Because of the interference of sunlight during day, we only use nighttime high-quality data. We further screen the data with extinction uncertainty and quality flags including CAD (cloud-aerosol discrimination) score, Ext_QC (extinction quality control flag), and AVD (atmospheric volume description). In this study, we only consider cloud-free retrievals and use aerosol layers with Ext_QC values of 0, 1, 18, and 16,

30   and CAD scores between -20 and -100. For the comparison, observations are averaged over the model grid, and the model results are sampled to only use days and grids when CALIOP data are available.

Both observations and model results show high extinction extended to 3 km close to Africa, descending to below 1 km when crossing the Atlantic Ocean. Although the model in general captures the vertical distribution of the extinction, it tends to underestimate it at low altitude over both Africa and the ocean. The underestimation over Africa is opposite to the com-

parison with MODIS discussed above. The magnitude of the underestimation over ocean also exceeds the comparison with MODIS.

Fig. 7 also shows non-sampled model results (i.e., those for which no CALIOP data are available) covering the full period and the whole region. While having similar vertical distribution, the sampled results generally have higher extinction com-

5   pared with those non-sampled. This difference reflects the limited spatial and temporal coverage of CALIOP. While part of the sample bias is reduced in comparison with the sampled model results, the substantial remaining bias could be due to the narrow swath of CALIOP and the relatively coarse model resolution. Therefore, we only use the CALIOP data for qualitative evaluation of the vertical distribution in the model, in addition to constraints by MODIS and AERONET data.

4.1. Source regions of the dust arriving at Amazon basin

10   While it is well recognized that Saharan dust does reach the Amazon basin, there is an ongoing discussion about the relative importance of Bodélé dust as a dominant source (Abouchami et al., 2013; Koren et al., 2006; Kumar et al., 2014). We thus ran sensitive tests to check the influence of dust from four regions (see Fig. 2): northwest Sahara (17.5 °W–12.5 °E and 21 °–35 °N), northeast Sahara (12.5 °–40 °E and 21 °–35 °N), West Sahel (17.5 °W–12.5 °E and 13 °–21 °N), and Bodélé (12.5 °–40 ° E and 13 °–21 °N). Emissions from the above regions account for 35 %, 14 %, 8 % and 20 % of total dust emission during

15   Jan-Apr 2014, respectively.

Figure 8 shows the column burden of total dust and the contribution of these four regions over 120 °W–60 °E and 60 °S–60 °N during the Amazonian wet season. We find that more than half of the dust over Central America and Northern South America is from northwest Sahara, follow by the contribution of West Sahel (20-30 %). The emission from Bodélé is important in east Brazil (east of 45 °W and south of 0 °), but contributes less than 20 % of the total dust over other Amazonian

20   regions. Such a low contribution from Bodélé is in contrast with the results by Koren et al. (2006), who suggested that Bodélé emissions are the main source for the dust transported to the Amazon basin.

Figure 8 also gives the sensitivity of the contribution from the above regions to the corresponding emissions: $s_i^j = (c_i^j / \sum_j c_i^j)/(e^j / \sum_j e^j)$, where s_i^j is the sensitivity of dust at grid i to emissions from region j, c_i^j is dust concentration at grid i originated from region j, and e^j are dust emissions from region j. It shows that dust over the central Amazon is most

25   sensitive to emissions in West Sahel, followed by northwest Sahara. High sensitivity to Bodélé emissions is limited to eastern Brazil. Therefore even with doubled emissions, Bodélé would not dominate dust over the central Amazon.

However, there is also intra-seasonal variability for the sources of dust arriving at the central Amazon. We find that the trans-Atlantic transport of northwest Saharan dust moves further north in January compared with February-April. Consequently, the dust over the central Amazon is more sensitive to Bodélé emissions, which thus become the largest contributor

30   in January. This wide spatiotemporal variability in sources to some extent explains the divergence in the literature.

5. Aerosols in the Central Amazon

5.1. Chemical components of aerosols at ATTO

Figure 9 shows time series of observed and simulated aerosol mass concentrations at ATTO from Jan-Apr 2014. The observed aerosols had a mean concentration of 13±8.6 µg m^{-3}, dominated by coarse aerosols with a mean contribution of 90 %. The coarse aerosol contribution is at the higher end of the previously reported range (66–78 %) at nearby sites (Artaxo et al., 1990; Formenti et al., 2001). However, the coarse aerosols defined in the latter are aerosols with $dp > 2$ µm, in contrast with 1 µm as used in this work. Applying the same criterion would yield a mean contribution of 75 % from coarse aerosols at ATTO, consistent with the reported range. The model shows similar aerosol concentrations (11±9.1 µg m^{-3}) with $r = 0.75$, but has less contribution of coarse aerosols (54 %).

One reason for this difference is the missing sources of PBA particles in the model, which has been found to dominate the coarse aerosols at background conditions in previous studies (Formenti et al., 2001). The observed background concentrations for coarse aerosols are around 2.8 µg m^{-3} while the model shows only 0.27 µg m^{-3}, implying concentrations of about 2.5 µg m^{-3} for PBA at ATTO. This background is within the reported range of 1.2-3 µg m^{-3} for coarse particles excluding dust at nearby sites (Formenti et al., 2001; Pöschl et al., 2010) and over southern Amazon (~10 °S) (Fuzzi et al., 2007) during the wet season.

In addition, the model also shows a higher background for fine aerosols (2.8 µg m^{-3}) compared with observations (0.41 µg m^{-3}). The difference of 2.4 µg m^{-3} in fine aerosol concentrations could be explained by the model bias in SOA production, which dominates fine aerosol concentrations. Barkley et al. (2011) found that GEOS-Chem has underestimated hydroxyl concentrations while overestimating isoprene and its oxidation products over tropical South America. The mean concentration of SOA in the model is 3.0±0.85 µg m^{-3}, while measurements from AMS (aerosol mass spectrometry) show an average of 0.6 µg m^{-3} during the wet season (Chen et al., 2009). Correcting the bias in background for both coarse and fine aerosols would yield better agreement in the contribution of coarse aerosol while not degrading the comparison of total concentrations.

During the wet season, the model shows a mean concentration of 6.3 µg m^{-3} for dust, 91 % of which are in coarse mode. It contributes to 59 % and 85-92 % of total aerosol mass on average and during dusty periods, respectively. We find that model dust correlates well with observed coarse aerosols ($r = 0.73$), indicating strong influence of dust on the observed variation of coarse aerosols. The two highest peaks on 18-19 Feb and 5-9 March (with dust concentrations up to 30-50 µg m^{-3}) could also be expected from the daily distribution of trans-Atlantic AOD in Fig.6, again implying the long range transport of dust from Africa to the ATTO site.

Model sea salt has a mean concentration of 0.31 µg m^{-3} and accounts for about 3 % of total aerosol mass on average. There is a moderate correlation ($r = 0.49$) between model sea salt and dust. Previous studies also show mixed transport of marine aerosol and dust to the Amazon basin with sea salt contribution of up to 10 % (Artaxo et al., 1990; Ben-Ami et al., 2010; Formenti et al., 2001; Talbot et al., 1990).

After correcting the bias in SOA concentrations, OA has a mean concentration of 1.3±1.6 μg m^{-3} and is still the largest contributor (54 %) to fine aerosols, followed by fine dust (23 %), sulfate-nitrate-ammonium (11 %), fine sea salt (9.4 %) and BC (2.8 %). The low sulfate contribution (3 % of total aerosol mass) is consistent with previous results (Talbot et al., 1990). Simulated POA has a mean concentration of 0.70±0.91 μg m^{-3} and could explain 50 % of observed variance of fine aerosol.

POA is generally present with co-emitted BC, with $r = 0.99$ in the model. Figure 10 shows time series of observed rBC from the SP2 and simulated BC during Jan-Apr 2014. Observed rBC has a background concentration of 1.8 ng m^{-3}. This "clean" condition is frequently interrupted and thus has median and 75th percentile concentrations of 16 and 53 ng m^{-3}, respectively. There are two peaks with observed BC higher than 100 ng m^{-3} on 8-9 March and 9-11 April. The model reproduced well the observed variation with r of 0.73, but generated a higher background concentration of 28 ng m^{-3}. The linear regression analysis between model and rBC also indicates a positive bias of 26 ng m^{-3} in simulated background concentrations. Source attribution in the model shows that open fires make a median contribution of 39 % (14 % and 68 % for 25th and 75th percentile) and account for most of the variance. The overestimate in the background is probably driven by fossil fuel combustion BC in the model, mainly from NSA. Figure 10 also shows that open fire in NSA and NAF are equally important for BC at ATTO during Jan-Apr 2014, with the latter becoming more important in the late wet season.

It is interesting to note that BC peaks generally coincide with coarse aerosol peaks, with r of 0.70 and 0.52 in the observed and simulated data, respectively. Long-range transport of dust mixed with open fire aerosols from Africa to the Amazon basin has been reported in previous studies (Baars et al., 2011; Ben-Ami et al., 2010; Guyon et al., 2003b; Rizzo et al., 2013; Talbot et al., 1990). Source attribution in the model, however, also points out events of African dust mixed with NSA fire plumes, which is consistent with the HYSPLIT back trajectories passing over NSA fire spots to the East/Northeast of ATTO (Andreae et al., 2015).

Figure 11 shows scatterplots of observed and simulated BC vs. CO concentrations for high BC events in Fig. 10 (cases a-e). Both, observations and model results show good correlation between CO and BC during those events, with r of 0.52-0.91 and 0.93-0.99, respectively, implying similar origin for the two species. The model captured the observed slope for case (c) well, but underestimated it for cases (d) and (e) by 30 % and 60 %, respectively.

Because of the relatively longer lifetime of CO in the atmosphere, the enhancement ratio of BC versus CO can indicate the age of an air mass, with lower ratios in more aged air. Assuming first order removal of BC, the age of an air mass can be estimated using Eq. (1):

$$t = -L * \ln \frac{f}{f_e}, \tag{1}$$

where L is the lifetime of BC, f is enhancement ratio of BC versus CO, and f_e is the emission ratio of BC versus CO from sources. For this calculation, we average f_e from the FINN inventory over NSA and NAF during Jan-Apr 2014. The derived f_e is 7.7±0.76 and 8.3±0.75 ng m^{-3} ppb^{-1} for open fires in NSA and NAF, respectively. For cases (a)-(c), the model shows a dominant contribution from NSA open fire with a simulated BC lifetime of 3.1 days. The corresponding age of the air mass is 1-3 days for the simulated peaks. For case (d), the model shows a dominant contribution from NAF open fires. Applying a

simulated BC lifetime of 5.6 days for NAF open fires, we derive a corresponding age of air mass of 11 days, consistent with the range of 8-12 d for the transport time of African plumes arriving in South America estimated by Ben-Ami et al. (2010). Model source attribution for case (e) indicates a combined contribution from NAF (80 %) and NSA (20 %) open fires for BC. Thus the slope in case (e) is also a similar combination of case (d) and case (a-c). The above calculation implies an infi-

5 nite lifetime for CO. Applying an average CO lifetime of two month against oxidation by the hydroxyl radical (Fisher et al., 2010), less than 20 % of CO would be lost at a timescale of 11 days. Accounting for this CO loss, the derived transport time would be increased by 10 %.

The difference between observed and simulated slopes could be due to variation in emission ratios from individual fires. The variation (10 %) in the emission factors for NSA and NAF fires from the FINN inventory is relatively small as they are

10 already averaged for different land cover/vegetation type. The uncertainty could be much larger accounting for individual fires. For example, the emission ratio of BC to CO reported by Andreae and Merlet (2001) has an uncertainty of 50 % for savanna and grassland fires, which would result in 50 % variation in the slope. The difference in aerosol removal time could also contribute to the bias in the slopes. As discussed in Sect. 4, the simulated aerosol lifetime is 14 % shorter than that derived from MODIS AOD over the ocean, which could result in a difference around 30 % in the slope. It is also possible that

15 the observed slope for case (e) is due to fires nearby, which are missed or underestimated in the model. Also, model results are for average conditions and individual cases may be quite different from the average.

5.2. Aerosol absorption at ATTO

Figure 12 shows time series of observed and simulated aerosol absorption at 550 nm and 400 nm at ATTO during Jan-Apr 2014. The observed absorption has a mean value of 1.5 ± 1.5 and 2.3 ± 2.3 Mm^{-1} at wavelengths of 550 and 400 nm, respective-

20 ly. The highest absorption is found in early January, with values higher than 10 Mm^{-1} at 550 nm. The simulated absorption at 550 and 400 nm is 1.3 ± 1.2 and 2.3 ± 2.2 Mm^{-1}, respectively, agreeing with the observations with an r of 0.64-0.66.

The model absorption is further separated into BC, BrC, and dust in Fig. 12. BC contributes 63 % of the absorption at 550 nm, followed by BrC (27 %, mainly from open fires) and dust (10 %) on average. The contribution of BrC to total carbona-ceous aerosol absorption (25 ± 8.8 %) is within the range 20-40 % on a global scale proposed by previous authors (Chung et

25 al., 2012b; Saleh et al., 2015; Wang et al., 2014b). Although the mean contribution is small, dust could occasionally be im-portant. One such example occurred in early March, as expected from Fig. 9, with a dust contribution of up to 50 %. Due to stronger wavelength dependence, relatively higher contribution to absorption at 400 nm is found from BrC (41 %) and dust (17 %) compared to the absorption at 550 nm.

Figure 13 shows scatterplots of absorption at 550 nm and 400 nm vs. BC concentrations during the same period. There is

30 high correlation between observed absorption at both wavelengths and SP2 rBC data with r of 0.96-0.98, implying a major contribution of BC and/or species with similar origin, such as BrC, consistent with the model source attribution of the aero-sol absorption discussed above. The slope increases from 0.023 for absorption at 550 nm to 0.038 for absorption at 400 nm,

reflecting the strong wavelength dependence of BrC absorption. We find that the model successfully captures observed correlation and slopes at both wavelengths.

Observed and simulated AAE during the period have mean values of 1.3±0.33 and 1.6±0.37, respectively. One uncertainty in the AAE estimation is due to its wavelength dependence. AAE estimated directly from Aethalometer data at 370 and 520 nm is 1.5±0.42, which is slightly higher than the value (1.3±0.33) based on a linear fit of multiple wavelength absorption. In addition, Rizzo et al. (2011) reported a typical uncertainty of 20 % in Aethalometer AAE, mainly due to the choice of scattering Ångström exponent.

Note that the contribution from BrC is directly affected by the OA/OC ratio assumed for POA in the model. In this work, we adopt a ratio of 1.7 measured in the Amazon basin during the wet season of 2008 (Chen et al., 2009), which is lower than the value of 2.1±0.2 for aged aerosol suggested by Turpin and Lim (2001). Using the latter ratio would increase BrC and total aerosol absorption at 550 nm by 25 % and 6 % at ATTO during the wet season. The corresponding AAE would also be increased to 1.7±0.37.

5.3. Aerosol light absorption in the Amazon basin

Figure 14 shows the distribution of simulated AAOD at 550 nm between 80 °W-35 °W and 24 °S-8 °N averaged over Jan-Apr 2014. During the wet season, AAOD over most of the Amazon region including the ATTO site is lower than 0.002. This low value reflects a minimal influence of human activities over the region, in contrast to the rest of the South American continent. High AAOD over Colombia is caused by open fires, whereas over Southern Brazil it originates from fuel combustion. Figure 14 also shows the separate contributions from BC, BrC, and dust to total absorption. We find that more than 50 % of AAOD is from BC except for Guyana, Suriname, French Guiana and northern Brazil, where the influence of dust becomes significant with up to 35 %. However, the dust influence, which could represent the influence of African plumes, becomes negligible for regions south of 10 °S. The contribution of BrC is generally between 20-30 %, and could be up to 40 % when it is more affected by open fires, such as in Colombia and Venezuela.

Figure 15 shows model AAE estimated from wavelength 550 and 400 nm over the Amazon basin for the period of Jan-Apr 2014. Simulated AAE values cover a wide range from ~1 to more than 2. The distribution of AAE indicates the distribution of LAA types over the Basin. The regions with AAE less than 1 are fossil fuel combustion dominated, while the regions with AAE higher than 1.5 are more affected by open fires and dust.

Note that the model bias in SOA production does not affect the simulated absorption, as the contribution of SOA to brown carbon is not accounted for. A recent study by Lambe et al. (2013) shows that the absorptivity of SOA depends on both precursor type and oxidation level. The derived MAE at 405 nm is less than 0.02 m^2 g^{-1} for biogenic SOA and less than 0.08 m^2 g^{-1} for aromatic SOA. These values are one to two orders of magnitude smaller than those for biofuel and open fires (1.4 and 1.3 m^2 g^{-1}, respectively). Adding SOA absorption using the upper limit values only increases total absorption at 400 nm by less than 8 % over the Amazon basin. The influence is even smaller if we correct the model positive bias in SOA production to be consistent with observations in the Amazon basin.

Due to limited information on the detailed components/concentrations of PBA and associated absorptivity (Despres et al., 2012), the contribution of PBA to absorption is not accounted for in the above results. However, assuming that the background of absorption at 550 nm is from PBA due to its relatively constant concentrations (Huffman et al., 2013; Pauliquevis et al., 2012), we obtain an absorption of 0.2 Mm^{-1} from observations at ATTO for PBA, accounting for 13 % of total absorption at 550 nm on average. This value is consistent with the intercept (0.24 Mm^{-1}) of the regression line between the absorption at 550 nm and the SP2 data in Fig.13, which can represent the upper limit assuming all absorption not correlated with rBC is from PBA. Our estimate is also consistent with Pauliquevis et al. (2012), who reported an average background of 50 ng m^{-3} of equivalent black carbon (BC$_e$), corresponding to an absorption around 0.3 Mm^{-1} for PBA in the central Amazon.

Assuming well-mixed PBA below a height of 2 km with absorption of 0.2 Mm^{-1}, we find that PBA could account for 5-40 % of total AAOD at 550 nm over the Amazon basin, with relatively lower contributions over regions with more influence from open fires (e.g., the northern Amazon). This estimate is roughly consistent with the results of Guyon et al. (2004), who reported 35-47 % of absorption attributed to biogenic particles during the wet-to-dry/wet season in the Amazon Basin.

6. Conclusion

We used the GEOS-Chem chemical transport model to interpret observed aerosol concentrations and associated absorption over the Amazon basin during Jan-Apr 2014. To better understand the source types and contributions to light absorbing aerosols and their optical properties over the Amazon basin, we modified the aerosol optical properties in the model to account for the coating enhancement of BC light absorption. We also added brown carbon as light absorber with its absorptivity depending on emission ratios of BC/OA based on the most recent study (Saleh et al., 2015). Our simulation used FINNv1.5 (Fire INventory from NCAR version 1.5) with daily resolution (Wiedinmyer et al., 2011) for open fire, so as to capture the observed daily variance over the Amazon basin.

The observations show relatively low aerosol concentrations and light absorption over the Amazon basin during the wet season. However, this low background is frequently interrupted by sources not fully quantified previously. Several studies have reported long-range transport of dust plumes from Africa to the Amazon basin during the wet season (Baars et al., 2011; Ben-Ami et al., 2010; Formenti et al., 2001). To investigate the influence of the trans-Atlantic transported plumes, we first evaluated the emissions and optical properties of dust over Africa through comparison with AERONET and MODIS AOD data. The comparison shows slightly positive model bias (~20 %) in dust AOD over Africa. Comparison with dust optical properties derived from Mie calculation using long-term AERONET observations suggests that the bias is mainly due to positive model bias (18 %) in the mass extinction efficiency (MEE) of dust. The comparison also indicates consistence between simulated mass absorption efficiency (MAE) and MAE derived from AERONET data.

We further examined the simulated trans-Atlantic transport constrained by MODIS and CALIOP observations. We find that GEOS-Chem reproduces well the spatial/vertical distribution as well as the time variance of the African outflows. Based on the gradient of the logarithm of the AOD over the Atlantic Ocean, we estimated a lifetime of dust of 3.2 d in the model, which is slightly underestimated (14 %) when compared with MODIS data (3.7 d). This comparison is better than in the

study by Ridley et al. (2012), probably due to difference in meteorology and updates in wet scavenging taken from the previous study by Wang et al. (2014a).

During Jan-Apr 2014, both the model and MODIS observations show five events of trans-Atlantic transport plumes from Africa to the Amazon basin. Model sensitivity test against sources show that dust over most of the Amazon basin is dominated by emissions from northwest Sahara, followed by the contribution from West Sahel during the period. On the other hand, the Bodélé emissions can dominate the dust over the Amazon basin in January and in eastern Brazil over the whole period.

Finally, we evaluated the model performance in the Amazon basin through comparison with observations at the ATTO site, which represents the Amazon basin with minimal human perturbation (Andreae et al., 2015). The observations show an average aerosol concentration of 13 ± 8.6 µg m^{-3} for the study period, 90 % of which is from coarse aerosol. The model is able to reproduce the mean concentrations (11 ± 9.1 µg m^{-3} with $r = 0.75$) but has less contribution from coarse aerosols. Detailed analysis indicates a positive model bias of 2.4 µg m^{-3} in SOA production and a missing source of primary biogenic aerosol (PBA) of 2.5 µg m^{-3}.

Source attribution in the model suggests that open fires are responsible for most variance of observed aerosol concentrations (BC in particular). Open fires from both northern South America and northern Africa are comparably important, with the latter more important in the late wet season. Based on the enhancement ratio of BC versus CO, fire emissions from northern South America generally arrive at ATTO within 1-3 d, whereas those from Africa have a transport time of 11 d, consistent with the range of 8-12 d found by Ben-Ami et al. (2010).

With modified optical properties, the model reproduces the observed light absorption and its wavelength dependence. The simulated Absorption Ångström exponent (AAE) of 1.6 ± 0.37 for total aerosols is within the uncertain range of AAE (1.5 ± 0.42) estimated directly from the Aethalometer data at 370 and 520 nm. Source attribution indicates a soot BC contribution of 63 %, followed by brown carbon (27 %) and dust (10 %) to the total absorption at 550 nm.

Expanding the model results to the Amazon basin, we find more than 50 % of total absorption at 550 nm is from BC except for Guyana, Suriname, French Guiana and northernmost Brazil, where the influence of dust becomes significant with up to 35 %. The brown carbon contribution is generally between 20-30 %. The spatial distribution of AAE suggests more fossil fuel combustion in the southern part of the Amazon (with AAE ~1), whereas more open fire and dust influence is found in the northern part of the basin (with AAE > 1.8).

In this study, we only considered OA from biofuel and open fires as brown carbon. Therefore, the model bias in SOA production as well as the missing representation of PBA does not affect the model results in total absorption. However, we also discussed the uncertainties of absorption due to SOA and PBA in the Amazon basin. Applying the upper limit of the MAE value for SOA, we find a difference of less than 8 % in absorption at 400 nm over the Amazon basin, even with the positive model bias in SOA production. Absorption due to PBA is important under background conditions. Assuming all background absorption of 0.2 Mm^{-1} at 550 nm is due to PBA, we find that PBA contributes 13 % of absorption at 550 nm

averaged over the whole wet season at ATTO site. Applying this constant background absorption to the whole Amazon basin and boundary layer, PBA could account for 5-40 % of total AAOD at 550 nm over the central Amazon.

Acknowledgments. The work has been supported by the Max Planck Society (MPG). We acknowledge the support by the Instituto Nacional de Pesquisas da Amazônia (INPA). We would like to thank all the people involved in the technical, logistical, and scientific support of the ATTO project, in particular Jürgen Kesselmeier, Reiner Ditz, Matthias Sörgel, Thomas Disper, Uwe Schultz, Steffen Schmidt, Thomas Seifert, Andrew Crozier, Antonio Ocimar Manzi, Hermes Braga Xavier, Elton Mendes da Silva, Nagib Alberto de Castro Souza, Adir Vasconcelos Brandão, Amauri Rodrigués Perreira, Antonio Huxley Melo Nascimento, Thiago de Lima Xavier, Josué Ferreira de Souza, Roberta Pereira de Souza, Bruno Takeshi, and Wallace Rabelo Costa. We acknowledge the support by the German Federal Ministry of Education and Research (BMBF contract 01LB1001A) and the Brazilian Ministério da Ciência, Tecnologia e Inovação (MCTI/FINEP contract 01.11.01248.00) as well as the Amazon State University (UEA), FAPEAM, LBA/INPA and SDS/CEUC/RDS-Uatumã. We thank the AERONET staff for their effort in establishing and maintaining the AERONET sites used in this study. The MODIS data were obtained from NASA Goddard Data Center and CALIPSO data were obtained from the NASA Langley Research Center Atmospheric Sciences Data Center. This paper contains results of research conducted under the Technical/Scientific Cooperation Agreement between the National Institute for Amazonian Research, Amazonas State University, and the Max-Planck-Gesellschaft e.V. The work was conducted under scientific licenses 001030/2012-4, 001262/2012-2, and 00254/2013-9 of the Brazilian National Council for Scientific and Technological Development (CNPq). The opinions expressed herein are the entire responsibility of the authors and not of the participating institutions.

References

Abouchami, W., Näthe, K., Kumar, A., Galer, S. J. G., Jochum, K. P., Williams, E., Horbe, A. M. C., Rosa, J. W. C., Balsam, W., Adams, D., Mezger, K., and Andreae, M. O.: Geochemical and isotopic characterization of the Bodélé Depression dust source and implications for transatlantic dust transport to the Amazon Basin, Earth Planet. Sci. Lett., 380, 112-123, doi:10.1016/j.epsl.2013.08.028, 2013.

Andreae, M. O., and Merlet, P.: Emission of trace gases and aerosols from biomass burning, Global Biogeochem. Cycles, 15, 955-966, 2001.

Andreae, M. O., and Gelencsér, A.: Black carbon or brown carbon? The nature of light-absorbing carbonaceous aerosols, Atmos. Chem. Phys., 6, 3131-3148, doi:10.5194/acp-6-3131-2006, 2006.

Andreae, M. O.: Aerosols Before Pollution, Science, 315, 50-51, doi:10.1126/science.1136529, 2007.

Andreae, M. O., and Ramanathan, V.: Climate's Dark Forcings, Science, 340, 280-281, doi:10.1126/science.1235731, 2013.

Andreae, M. O., Acevedo, O. C., Araùjo, A., Artaxo, P., Barbosa, C. G. G., Barbosa, H. M. J., Brito, J., Carbone, S., Chi, X., Cintra, B. B. L., da Silva, N. F., Dias, N. L., Dias-Júnior, C. Q., Ditas, F., Ditz, R., Godoi, A. F. L., Godoi, R. H. M., Heimann, M., Hoffmann, T., Kesselmeier, J., Könemann, T., Krüger, M. L., Lavric, J. V., Manzi, A. O., Lopes, A. P., Martins, D. L., Mikhailov, E. F., Moran-Zuloaga, D., Nelson, B. W., Nölscher, A. C., Santos Nogueira, D., Piedade, M. T. F., Pöhlker, C., Pöschl, U., Quesada, C. A., Rizzo, L. V., Ro, C. U., Ruckteschler, N., Sá, L. D. A., de Oliveira Sá, M., Sales, C. B., dos Santos, R. M. N., Saturno, J., Schöngart, J., Sörgel, M., de Souza, C. M., de Souza, R. A. F., Su, H., Targhetta, N., Tóta, J., Trebs, I., Trumbore, S., van Eijck, A., Walter, D., Wang, Z., Weber, B., Williams, J., Winderlich, J., Wittmann, F., Wolff, S., and Yáñez-Serrano, A. M.: The Amazon Tall Tower Observatory (ATTO): overview of pilot measurements on ecosystem ecology, meteorology, trace gases, and aerosols, Atmos. Chem. Phys., 15, 10723-10776, doi:10.5194/acp-15-10723-2015, 2015.

Artaxo, P., Maenhaut, W., Storms, H., and Van Grieken, R.: Aerosol characteristics and sources for the Amazon Basin during the wet season, J. Geophys. Res., 95, 16971-16985, doi:10.1029/JD095iD10p16971, 1990.

Baars, H., Ansmann, A., Althausen, D., Engelmann, R., Artaxo, P., Pauliquevis, T., and Souza, R.: Further evidence for significant smoke transport from Africa to Amazonia, Geophys. Res. Lett., 38, doi:10.1029/2011GL049200, 2011.

Bahadur, R., Praveen, P. S., Xu, Y., and Ramanathan, V.: Solar absorption by elemental and brown carbon determined from spectral observations, P. Natl. Acad. Sci. USA, 109, 17366-17371, doi:10.1073/pnas.1205910109, 2012.

Barkley, M. P., Palmer, P. I., Ganzeveld, L., Arneth, A., Hagberg, D., Karl, T., Guenther, A., Paulot, F., Wennberg, P. O., Mao, J., Kurosu, T. P., Chance, K., Müller, J. F., De Smedt, I., Van Roozendael, M., Chen, D., Wang, Y., and Yantosca, R. M.: Can a "state of the art" chemistry transport model simulate Amazonian tropospheric chemistry?, J. Geophys. Res., 116, n/a-n/a, doi:10.1029/2011JD015893, 2011.

Ben-Ami, Y., Koren, I., Rudich, Y., Artaxo, P., Martin, S. T., and Andreae, M. O.: Transport of North African dust from the Bodélé depression to the Amazon Basin: a case study, Atmos. Chem. Phys., 10, 7533-7544, doi:10.5194/acp-10-7533-2010, 2010.

Bond, T. C., and Bergstrom, R. W.: Light absorption by carbonaceous particles: An investigative review, Aerosol Sci. Technol., 40, 27-67, doi:10.1080/02786820500421521, 2006.

Bond, T. C., Bhardwaj, E., Dong, R., Jogani, R., Jung, S. K., Roden, C., Streets, D. G., and Trautmann, N. M.: Historical emissions of black and organic carbon aerosol from energy-related combustion, 1850-2000, Global Biogeochem. Cycles, 21, Gb2018, doi:10.1029/2006gb002840, 2007.

Bond, T. C., Doherty, S. J., Fahey, D. W., Forster, P. M., Berntsen, T., DeAngelo, B. J., Flanner, M. G., Ghan, S., Kärcher, B., Koch, D., Kinne, S., Kondo, Y., Quinn, P. K., Sarofim, M. C., Schultz, M. G., Schulz, M., Venkataraman, C., Zhang, H., Zhang, S., Bellouin, N., Guttikunda, S. K., Hopke, P. K., Jacobson, M. Z., Kaiser, J. W., Klimont, Z., Lohmann, U., Schwarz, J. P., Shindell, D., Storelvmo, T., Warren, S. G., and Zender, C. S.: Bounding the role of black carbon in the climate system: A scientific assessment, J. Geophys. Res., 118, 5380-5552, doi:10.1002/jgrd.50171, 2013.

Castro Videla, F., Barnaba, F., Angelini, F., Cremades, P., and Gobbi, G. P.: The relative role of Amazonian and non-Amazonian fires in building up the aerosol optical depth in South America: A five year study (2005–2009), Atmos. Res., 122, 298-309, doi:10.1016/j.atmosres.2012.10.026, 2013.

Chen, Q., Farmer, D. K., Schneider, J., Zorn, S. R., Heald, C. L., Karl, T. G., Guenther, A., Allan, J. D., Robinson, N., Coe, H., Kimmel, J. R., Pauliquevis, T., Borrmann, S., Poschl, U., Andreae, M. O., Artaxo, P., Jimenez, J. L., and Martin, S. T.: Mass spectral characterization of submicron biogenic organic particles in the Amazon Basin, Geophys. Res. Lett., 36, L20806, doi:10.1029/2009gl039880, 2009.

Chen, Q., Farmer, D. K., Rizzo, L. V., Pauliquevis, T., Kuwata, M., Karl, T. G., Guenther, A., Allan, J. D., Coe, H., Andreae, M. O., Pöschl, U., Jimenez, J. L., Artaxo, P., and Martin, S. T.: Submicron particle mass concentrations and sources in the Amazonian wet season (AMAZE-08), Atmos. Chem. Phys., 15, 3687-3701, doi:10.5194/acp-15-3687-2015, 2015.

Chung, C. E., Kim, S. W., Lee, M., Yoon, S. C., and Lee, S.: Carbonaceous aerosol AAE inferred from in-situ aerosol measurements at the Gosan ABC super site, and the implications for brown carbon aerosol, Atmos. Chem. Phys., 12, 6173-6184, doi:10.5194/acp-12-6173-2012, 2012a.

Chung, C. E., Ramanathan, V., and Decremer, D.: Observationally constrained estimates of carbonaceous aerosol radiative forcing, P. Natl. Acad. Sci. USA, 109, 11624-11629, doi:10.1073/pnas.1203707109, 2012b.

Chung, S. H., and Seinfeld, J. H.: Global distribution and climate forcing of carbonaceous aerosols, J. Geophys. Res., 107, 4407, doi:10.1029/2001jd001397, 2002.

Despres, V. R., Huffman, J. A., Burrows, S. M., Hoose, C., Safatov, A. S., Buryak, G., Frohlich-Nowoisky, J., Elbert, W., Andreae, M. O., Poschl, U., and Jaenicke, R.: Primary biological aerosol particles in the atmosphere: a review, Tellus Ser. B-Chem. Phys. Meteorol., 64, doi:10.3402/tellusb.v64i0.15598, 2012.

Drury, E., Jacob, D. J., Spurr, R. J. D., Wang, J., Shinozuka, Y., Anderson, B. E., Clarke, A. D., Dibb, J., McNaughton, C., and Weber, R.: Synthesis of satellite (MODIS), aircraft (ICARTT), and surface (IMPROVE, EPA-AQS, AERONET) aerosol observations over eastern North America to improve MODIS aerosol retrievals and constrain surface aerosol concentrations and sources, J. Geophys. Res., 115, D14204, doi:10.1029/2009jd012629, 2010.

Fairlie, T. D., Jacob, D. J., and Park, R. J.: The impact of transpacific transport of mineral dust in the United States, Atmos. Environ., 41, 1251-1266, doi:10.1016/j.atmosenv.2006.09.048, 2007.

Fisher, J. A., Jacob, D. J., Purdy, M. T., Kopacz, M., Le Sager, P., Carouge, C., Holmes, C. D., Yantosca, R. M., Batchelor, R. L., Strong, K., Diskin, G. S., Fuelberg, H. E., Holloway, J. S., Hyer, E. J., McMillan, W. W., Warner, J., Streets, D. G., Zhang, Q., Wang, Y., and Wu, S.: Source attribution and interannual variability of Arctic pollution in spring constrained by aircraft (ARCTAS, ARCPAC) and satellite (AIRS) observations of carbon monoxide, Atmos. Chem. Phys., 10, 977-996, doi:10.5194/acp-10-977-2010, 2010.

Formenti, P., Andreae, M. O., Lange, L., Roberts, G., Cafmeyer, J., Rajta, I., Maenhaut, W., Holben, B. N., Artaxo, P., and Lelieveld, J.: Saharan dust in Brazil and Suriname during the Large-Scale Biosphere-Atmosphere Experiment in

Amazonia (LBA) - Cooperative LBA Regional Experiment (CLAIRE) in March 1998, J. Geophys. Res., 106, 14919-14934, doi:10.1029/2000JD900827, 2001.

Fuzzi, S., Decesari, S., Facchini, M. C., Cavalli, F., Emblico, L., Mircea, M., Andreae, M. O., Trebs, I., Hoffer, A., Guyon, P., Artaxo, P., Rizzo, L. V., Lara, L. L., Pauliquevis, T., Maenhaut, W., Raes, N., Chi, X., Mayol-Bracero, O. L., Soto-García, L. L., Claeys, M., Kourtchev, I., Rissler, J., Swietlicki, E., Tagliavini, E., Schkolnik, G., Falkovich, A. H., Rudich, Y., Fisch, G., and Gatti, L. V.: Overview of the inorganic and organic composition of size-segregated aerosol in Rondônia, Brazil, from the biomass-burning period to the onset of the wet season, J. Geophys. Res., 112, n/a-n/a, doi:10.1029/2005JD006741, 2007.

Guenther, A., Karl, T., Harley, P., Wiedinmyer, C., Palmer, P. I., and Geron, C.: Estimates of global terrestrial isoprene emissions using MEGAN (Model of Emissions of Gases and Aerosols from Nature), Atmos. Chem. Phys., 6, 3181-3210, doi:10.5194/acp-6-3181-2006, 2006.

Guyon, P., Graham, B., Beck, J., Boucher, O., Gerasopoulos, E., Mayol-Bracero, O. L., Roberts, G. C., Artaxo, P., and Andreae, M. O.: Physical properties and concentration of aerosol particles over the Amazon tropical forest during background and biomass burning conditions, Atmos. Chem. Phys., 3, 951-967, doi:10.5194/acp-3-951-2003, 2003a.

Guyon, P., Graham, B., Roberts, G. C., Mayol-Bracero, O. L., Maenhaut, W., Artaxo, P., and Andreae, M. O.: In-canopy gradients, composition, sources, and optical properties of aerosol over the Amazon forest, J. Geophys. Res., 108, n/a-n/a, doi:10.1029/2003JD003465, 2003b.

Guyon, P., Graham, B., Roberts, G. C., Mayol-Bracero, O. L., Maenhaut, W., Artaxo, P., and Andreae, M. O.: Sources of optically active aerosol particles over the Amazon forest, Atmos. Environ., 38, 1039-1051, doi:10.1016/j.atmosenv.2003.10.051, 2004.

Henze, D. K., and Seinfeld, J. H.: Global secondary organic aerosol from isoprene oxidation, Geophys. Res. Lett., 33, L09812, doi:10.1029/2006gl025976, 2006.

Henze, D. K., Seinfeld, J. H., Ng, N. L., Kroll, J. H., Fu, T. M., Jacob, D. J., and Heald, C. L.: Global modeling of secondary organic aerosol formation from aromatic hydrocarbons: high- vs. low-yield pathways, Atmos. Chem. Phys., 8, 2405-2420, 2008.

Huffman, J. A., Prenni, A. J., DeMott, P. J., Pöhlker, C., Mason, R. H., Robinson, N. H., Fröhlich-Nowoisky, J., Tobo, Y., Després, V. R., Garcia, E., Gochis, D. J., Harris, E., Müller-Germann, I., Ruzene, C., Schmer, B., Sinha, B., Day, D. A., Andreae, M. O., Jimenez, J. L., Gallagher, M., Kreidenweis, S. M., Bertram, A. K., and Pöschl, U.: High concentrations of biological aerosol particles and ice nuclei during and after rain, Atmos. Chem. Phys., 13, 6151-6164, doi:10.5194/acp-13-6151-2013, 2013.

IPCC: Climate Change 2013: The Physical Science Basis, Contribution of Working Group I to the Fifth Assessment Report of the Intergovernmental Panel on Climate Change, edited by: Stocker, T. F., Qin, D., Plattner, G.-K., Tignor, M., Allen, S. K., Boschung, J., Nauels, A., Xia, Y., Bex V. and Midgley, P.M., Cambridge University Press, Cambridge, United Kingdom and New York, NY, USA, 2013.

Jacobson, M. Z.: Strong radiative heating due to the mixing state of black carbon in atmospheric aerosols, Nature, 409, 695-697, 2001.

Jaeglé, L., Quinn, P. K., Bates, T. S., Alexander, B., and Lin, J. T.: Global distribution of sea salt aerosols: new constraints from in situ and remote sensing observations, Atmos. Chem. Phys., 11, 3137-3157, doi:10.5194/acp-11-3137-2011, 2011.

Kim, D., Chin, M., Yu, H., Diehl, T., Tan, Q., Kahn, R. A., Tsigaridis, K., Bauer, S. E., Takemura, T., Pozzoli, L., Bellouin, N., Schulz, M., Peyridieu, S., Chédin, A., and Koffi, B.: Sources, sinks, and transatlantic transport of North African dust aerosol: A multimodel analysis and comparison with remote sensing data, J. Geophys. Res., 119, 6259-6277, doi:10.1002/2013JD021099, 2014.

Kinne, S., Schulz, M., Textor, C., Guibert, S., Balkanski, Y., Bauer, S. E., Berntsen, T., Berglen, T. F., Boucher, O., Chin, M., Collins, W., Dentener, F., Diehl, T., Easter, R., Feichter, J., Fillmore, D., Ghan, S., Ginoux, P., Gong, S., Grini, A., Hendricks, J., Herzog, M., Horowitz, L., Isaksen, I., Iversen, T., Kirkevåg, A., Kloster, S., Koch, D., Kristjansson, J. E., Krol, M., Lauer, A., Lamarque, J. F., Lesins, G., Liu, X., Lohmann, U., Montanaro, V., Myhre, G., Penner, J., Pitari, G., Reddy, S., Seland, O., Stier, P., Takemura, T., and Tie, X.: An AeroCom initial assessment – optical properties in aerosol component modules of global models, Atmos. Chem. Phys., 6, 1815-1834, doi:10.5194/acp-6-1815-2006, 2006.

Koepke, P., Hess, M., Schult, I., and Shettle, E. P.: Global Aerosol Data Set, Report No. 243, Max-Planck-Institut fur Meteorologie, Hamburg, ISSN 0937-1060, 1997.

Koren, I., Kaufman, Y. J., Washington, R., Todd, M. C., Rudich, Y., Martins, J. V., and Rosenfeld, D.: The Bodélé depression: a single spot in the Sahara that provides most of the mineral dust to the Amazon forest, Environmental Research Letters, 1, 014005, 2006.

Kumar, A., Abouchami, W., Galer, S. J. G., Garrison, V. H., Williams, E., and Andreae, M. O.: A radiogenic isotope tracer study of transatlantic dust transport from Africa to the Caribbean, Atmos. Environ., 82, 130-143, doi:10.1016/j.atmosenv.2013.10.021, 2014.

Lambe, A. T., Cappa, C. D., Massoli, P., Onasch, T. B., Forestieri, S. D., Martin, A. T., Cummings, M. J., Croasdale, D. R., Brune, W. H., Worsnop, D. R., and Davidovits, P.: Relationship between Oxidation Level and Optical Properties of Secondary Organic Aerosol, Environ. Sci. Technol., 47, 6349-6357, doi:10.1021/es401043j, 2013.

Levy, R. C., Remer, L. A., Martins, J. V., Kaufman, Y. J., Plana-Fattori, A., Redemann, J., and Wenny, B.: Evaluation of the MODIS Aerosol Retrievals over Ocean and Land during CLAMS, J. Atmos. Sci., 62, 974-992, doi:doi:10.1175/JAS3391.1, 2005.

Lin, G., Penner, J. E., Flanner, M. G., Sillman, S., Xu, L., and Zhou, C.: Radiative forcing of organic aerosol in the atmosphere and on snow: Effects of SOA and brown carbon, J. Geophys. Res., 119, 7453-7476, doi:10.1002/2013JD021186, 2014.

Liu, H. Y., Jacob, D. J., Bey, I., and Yantosca, R. M.: Constraints from Pb-210 and Be-7 on wet deposition and transport in a global three-dimensional chemical tracer model driven by assimilated meteorological fields, J. Geophys. Res., 106, 12109-12128, 2001.

Martin, R. V., Jacob, D. J., Yantosca, R. M., Chin, M., and Ginoux, P.: Global and regional decreases in tropospheric oxidants from photochemical effects of aerosols, J. Geophys. Res., 108, 4097, doi:10.1029/2002JD002622, 2003.

Martin, S. T., Andreae, M. O., Althausen, D., Artaxo, P., Baars, H., Borrmann, S., Chen, Q., Farmer, D. K., Guenther, A., Gunthe, S. S., Jimenez, J. L., Karl, T., Longo, K., Manzi, A., Müller, T., Pauliquevis, T., Petters, M. D., Prenni, A. J., Pöschl, U., Rizzo, L. V., Schneider, J., Smith, J. N., Swietlicki, E., Tota, J., Wang, J., Wiedensohler, A., and Zorn, S. R.: An overview of the Amazonian Aerosol Characterization Experiment 2008 (AMAZE-08), Atmos. Chem. Phys., 10, 11415-11438, doi:10.5194/acp-10-11415-2010, 2010a.

Martin, S. T., Andreae, M. O., Artaxo, P., Baumgardner, D., Chen, Q., Goldstein, A. H., Guenther, A., Heald, C. L., Mayol-Bracero, O. L., McMurry, P. H., Pauliquevis, T., Pschl, U., Prather, K. A., Roberts, G. C., Saleska, S. R., Silva Dias, M. A., Spracklen, D. V., Swietlicki, E., and Trebs, I.: Sources and properties of Amazonian aerosol particles, doi:10.1029/2008RG000280, 2010b.

Martins, F. R., and Pereira, E. B.: Parameterization of aerosols from burning biomass in the Brazil-SR radiative transfer model, Solar Energy, 80, 231-239, doi:10.1016/j.solener.2005.03.008, 2006.

McConnell, C. L., Formenti, P., Highwood, E. J., and Harrison, M. A. J.: Using aircraft measurements to determine the refractive index of Saharan dust during the DODO Experiments, Atmos. Chem. Phys., 10, 3081-3098, doi:10.5194/acp-10-3081-2010, 2010.

Myhre, G., Samset, B. H., Schulz, M., Balkanski, Y., Bauer, S., Berntsen, T. K., Bian, H., Bellouin, N., Chin, M., Diehl, T., Easter, R. C., Feichter, J., Ghan, S. J., Hauglustaine, D., Iversen, T., Kinne, S., Kirkevåg, A., Lamarque, J. F., Lin, G., Liu, X., Lund, M. T., Luo, G., Ma, X., van Noije, T., Penner, J. E., Rasch, P. J., Ruiz, A., Seland, Ø., Skeie, R. B., Stier, P., Takemura, T., Tsigaridis, K., Wang, P., Wang, Z., Xu, L., Yu, H., Yu, F., Yoon, J. H., Zhang, K., Zhang, H., and Zhou, C.: Radiative forcing of the direct aerosol effect from AeroCom Phase II simulations, Atmos. Chem. Phys., 13, 1853-1877, doi:10.5194/acp-13-1853-2013, 2013.

Park, R. J., Jacob, D. J., Chin, M., and Martin, R. V.: Sources of carbonaceous aerosols over the United States and implications for natural visibility, J. Geophys. Res., 108, 4355, doi:10.1029/2002jd003190, 2003.

Park, R. J., Jacob, D. J., Palmer, P. I., Clarke, A. D., Weber, R. J., Zondlo, M. A., Eisele, F. L., Bandy, A. R., Thornton, D. C., Sachse, G. W., and Bond, T. C.: Export efficiency of black carbon aerosol in continental outflow: Global implications, J. Geophys. Res., 110, D11205, doi:10.1029/2004jd005432, 2005.

Pauliquevis, T., Lara, L. L., Antunes, M. L., and Artaxo, P.: Aerosol and precipitation chemistry measurements in a remote site in Central Amazonia: the role of biogenic contribution, Atmos. Chem. Phys., 12, 4987-5015, doi:10.5194/acp-12-4987-2012, 2012.

Pöschl, U., Martin, S. T., Sinha, B., Chen, Q., Gunthe, S. S., Huffman, J. A., Borrmann, S., Farmer, D. K., Garland, R. M., Helas, G., Jimenez, J. L., King, S. M., Manzi, A., Mikhailov, E., Pauliquevis, T., Petters, M. D., Prenni, A. J., Roldin, P., Rose, D., Schneider, J., Su, H., Zorn, S. R., Artaxo, P., and Andreae, M. O.: Rainforest Aerosols as Biogenic Nuclei of Clouds and Precipitation in the Amazon, Science, 329, 1513-1516, doi:10.1126/science.1191056, 2010.

Pye, H. O. T., Chan, A. W. H., Barkley, M. P., and Seinfeld, J. H.: Global modeling of organic aerosol: the importance of reactive nitrogen (NO_x and NO_3), Atmos. Chem. Phys., 10, 11261-11276, doi:10.5194/acp-10-11261-2010, 2010.

Ramanathan, V., and Carmichael, G.: Global and regional climate changes due to black carbon, Nature Geoscience, 1, 221-227, doi:10.1038/ngeo156, 2008.

Ridley, D. A., Heald, C. L., and Ford, B.: North African dust export and deposition: A satellite and model perspective, J. Geophys. Res., 117, doi:10.1029/2011JD016794, 2012.

Ridley, D. A., Heald, C. L., and Prospero, J. M.: What controls the recent changes in African mineral dust aerosol across the Atlantic?, Atmos. Chem. Phys., 14, 5735-5747, doi:10.5194/acp-14-5735-2014, 2014.

Rizzo, L. V., Artaxo, P., Karl, T., Guenther, A. B., and Greenberg, J.: Aerosol properties, in-canopy gradients, turbulent fluxes and VOC concentrations at a pristine forest site in Amazonia, Atmos. Environ., 44, 503-511, doi:10.1016/j.atmosenv.2009.11.002, 2010.

Rizzo, L. V., Correia, A. L., Artaxo, P., Procópio, A. S., and Andreae, M. O.: Spectral dependence of aerosol light absorption over the Amazon Basin, Atmos. Chem. Phys., 11, 8899-8912, doi:10.5194/acp-11-8899-2011, 2011.

Rizzo, L. V., Artaxo, P., Müller, T., Wiedensohler, A., Paixão, M., Cirino, G. G., Arana, A., Swietlicki, E., Roldin, P., Fors, E. O., Wiedemann, K. T., Leal, L. S. M., and Kulmala, M.: Long term measurements of aerosol optical properties at a primary forest site in Amazonia, Atmos. Chem. Phys., 13, 2391-2413, doi:10.5194/acp-13-2391-2013, 2013.

Rosário, N. E., Longo, K. M., Freitas, S. R., Yamasoe, M. A., and Fonseca, R. M.: Modeling the South American regional smoke plume: aerosol optical depth variability and surface shortwave flux perturbation, Atmos. Chem. Phys., 13, 2923-2938, doi:10.5194/acp-13-2923-2013, 2013.

Saleh, R., Marks, M., Heo, J., Adams, P. J., Donahue, N. M., and Robinson, A. L.: Contribution of brown carbon and lensing to the direct radiative effect of carbonaceous aerosols from biomass and biofuel burning emissions, J. Geophys. Res., n/a-n/a, doi:10.1002/2015JD023697-T, 2015.

Schmid, O., Artaxo, P., Arnott, W. P., Chand, D., Gatti, L. V., Frank, G. P., Hoffer, A., Schnaiter, M., and Andreae, M. O.: Spectral light absorption by ambient aerosols influenced by biomass burning in the Amazon Basin. I: Comparison and field calibration of absorption measurement techniques, Atmos. Chem. Phys., 6, 3443-3462, doi:10.5194/acp-6-3443-2006, 2006.

Schultz, M., Rast, S., van het Bolscher, M., Pulles, T., Brand, R., Pereira, J., Mota, B., Spessa, A., Dalsøren, S., van Nojie, T., and Szopa, S.: Emission data sets and methodologies for estimating emissions, RETRO project report D1-6, Hamburg, 2007.

Schulz, M., Textor, C., Kinne, S., Balkanski, Y., Bauer, S., Berntsen, T., Berglen, T., Boucher, O., Dentener, F., Guibert, S., Isaksen, I. S. A., Iversen, T., Koch, D., Kirkevag, A., Liu, X., Montanaro, V., Myhre, G., Penner, J. E., Pitari, G., Reddy, S., Seland, O., Stier, P., and Takemura, T.: Radiative forcing by aerosols as derived from the AeroCom present-day and pre-industrial simulations, Atmos. Chem. Phys., 6, 5225-5246, 2006.

Sinyuk, A., Torres, O., and Dubovik, O.: Combined use of satellite and surface observations to infer the imaginary part of refractive index of Saharan dust, Geophys. Res. Lett., 30, n/a-n/a, doi:10.1029/2002GL016189, 2003.

Swap, R., Garstang, M., Greco, S., Talbot, R., and Kållberg, P.: Saharan dust in the Amazon Basin, Tellus B, 44, doi:10.3402/tellusb.v44i2.15434, 2011.

Talbot, R. W., Andreae, M. O., Berresheim, H., Artaxo, P., Garstang, M., Harriss, R. C., Beecher, K. M., and Li, S. M.: Aerosol chemistry during the wet season in central Amazonia: The influence of long-range transport, J. Geophys. Res., 95, 16955-16969, doi:10.1029/JD095iD10p16955, 1990.

Turpin, B. J., and Lim, H. J.: Species contributions to PM2.5 mass concentrations: Revisiting common assumptions for estimating organic mass, Aerosol Sci. Technol., 35, 602-610, 2001.

Wang, J., Christopher, S. A., Brechtel, F., Kim, J., Schmid, B., Redemann, J., Russell, P. B., Quinn, P., and Holben, B. N.: Geostationary satellite retrievals of aerosol optical thickness during ACE-Asia, J. Geophys. Res., 108, n/a-n/a, doi:10.1029/2003JD003580, 2003a.

Wang, J., Christopher, S. A., Reid, J. S., Maring, H., Savoie, D., Holben, B. N., Livingston, J. M., Russell, P. B., and Yang, S.-K.: GOES 8 retrieval of dust aerosol optical thickness over the Atlantic Ocean during PRIDE, J. Geophys. Res., 108, n/a-n/a, doi:10.1029/2002JD002494, 2003b.

Wang, Q., Jacob, D. J., Fisher, J. A., Mao, J., Leibensperger, E. M., Carouge, C. C., Le Sager, P., Kondo, Y., Jimenez, J. L., Cubison, M. J., and Doherty, S. J.: Sources of carbonaceous aerosols and deposited black carbon in the Arctic in winter-spring: implications for radiative forcing, Atmos. Chem. Phys., 11, 12453-12473, doi:10.5194/acp-11-12453-2011, 2011.

Wang, Q., Jacob, D. J., Spackman, J. R., Perring, A. E., Schwarz, J. P., Moteki, N., Marais, E. A., Ge, C., Wang, J., and Barrett, S. R. H.: Global budget and radiative forcing of black carbon aerosol: Constraints from pole-to-pole (HIPPO) observations across the Pacific, J. Geophys. Res., 119, 2013JD020824, doi:10.1002/2013JD020824, 2014a.

Wang, X., Heald, C. L., Ridley, D. A., Schwarz, J. P., Spackman, J. R., Perring, A. E., Coe, H., Liu, D., and Clarke, A. D.: Exploiting simultaneous observational constraints on mass and absorption to estimate the global direct radiative forcing of black carbon and brown carbon, Atmos. Chem. Phys., 14, 10989-11010, doi:10.5194/acp-14-10989-2014, 2014b.

Wang, Y. H., Jacob, D. J., and Logan, J. A.: Global simulation of tropospheric O-3-NOx-hydrocarbon chemistry 1. Model formulation, J. Geophys. Res., 103, 10713-10725, doi:10.1029/98jd00158, 1998.

Wesely, M. L.: Parameterization of surface resistances to gaseous dry deposition in regional-scale numerical-models, Atmos. Environ., 23, 1293-1304, doi:10.1016/0004-6981(89)90153-4, 1989.

Wiedinmyer, C., Akagi, S. K., Yokelson, R. J., Emmons, L. K., Al-Saadi, J. A., Orlando, J. J., and Soja, A. J.: The Fire INventory from NCAR (FINN): a high resolution global model to estimate the emissions from open burning, Geosci. Model Dev., 4, 625-641, doi:10.5194/gmd-4-625-2011, 2011.

Winderlich, J., Chen, H., Gerbig, C., Seifert, T., Kolle, O., Lavrič, J. V., Kaiser, C., Höfer, A., and Heimann, M.: Continuous low-maintenance CO2/CH4/H2O measurements at the Zotino Tall Tower Observatory (ZOTTO) in Central Siberia, Atmos. Meas. Tech., 3, 1113-1128, doi:10.5194/amt-3-1113-2010, 2010.

Young, S. A., and Vaughan, M. A.: The Retrieval of Profiles of Particulate Extinction from Cloud-Aerosol Lidar Infrared Pathfinder Satellite Observations (CALIPSO) Data: Algorithm Description, Journal of Atmospheric and Oceanic Technology, 26, 1105-1119, doi:doi:10.1175/2008JTECHA1221.1, 2009.

Yu, H., Chin, M., Yuan, T., Bian, H., Remer, L. A., Prospero, J. M., Omar, A., Winker, D., Yang, Y., Zhang, Y., Zhang, Z., and Zhao, C.: The fertilizing role of African dust in the Amazon rainforest: A first multiyear assessment based on data from Cloud-Aerosol Lidar and Infrared Pathfinder Satellite Observations, Geophys. Res. Lett., 42, 1984-1991, doi:10.1002/2015GL063040, 2015.

Zender, C. S., Bian, H., and Newman, D.: Mineral Dust Entrainment and Deposition (DEAD) model: Description and 1990s dust climatology, J. Geophys. Res., 108, n/a-n/a, doi:10.1029/2002JD002775, 2003.

Zhang, L. M., Gong, S. L., Padro, J., and Barrie, L.: A size-segregated particle dry deposition scheme for an atmospheric aerosol module, Atmos. Environ., 35, 549-560, doi:10.1016/s1352-2310(00)00326-5, 2001.

Table 1: Optical properties of light absorbing aerosol at 550 nm in GEOS-Chem

Type			Density (g cm^{-3})	Refractive Index	MAE[a] (m^2 g^{-1})	AAE[b]
Black carbon	Base		1.8	1.95-0.79i	5.9	1.3
	Update		1.8	1.95-0.79i	12	0.5
Organic carbon	Base		1.3	1.53-0.006i	0.16	0.8
	Update	Biofuel	1.3	1.7-0.023i	0.66	2.5
		Open Fire	1.3	1.7-0.017i	0.5	3.1
Dust	Base		2.5-2.65	1.56-0.0014i		
	Update		2.5-2.65	1.56-0.0014i		

[a] Mass absorption efficiency
[b] Absorption Ångström exponent, estimated between wavelength of 400 and 550 nm

Table 2: GEOS-Chem emissions of carbonaceous aerosols in Jan-Apr 2014.

Regions	Black Carbon (Tg a^{-1})		Organic Aerosols[a] (Tg a^{-1})		
	Fuel[b]	Open Fire[c]	Fuel[b]	Open Fire[c]	SOA[d]
North America (170–17.5 °W, 24–88 °N)	0.42 (12 %)	0.03	1.12 (44 %)	0.64	0.54 (84 %)
Central America (107–61 °W, 0–24 °N)	0.13 (23 %)	0.18	0.64 (48 %)	2.84	1.90 (11 %)
Northern South America (61–45 ° W, 0–10 ° N & 82–34.5 °W, 24–0 °S)	0.18 (34 %)	0.04	0.63 (71 %)	0.70	4.06 (3 %)
Southern South America (76–45 °W, 56–24 ° S)	0.09 (30 %)	0.01	0.27 (65 %)	0.22	0.52 (7 %)
Europe (10 °W –40 °E, 37.5–71 °N)	0.55 (18 %)	0.02	1.55 (62 %)	0.29	0.30 (46 %)
Northern Africa (17.5 °W –40 °E, 15 –37.5 °N & 17.5 °W–52 °E, 0–15 °N)	0.32 (63 %)	0.62	1.50 (82 %)	10.65	6.40 (9 %)
Southern Africa (8 –51 °E, 35–0 °S)	0.16 (69 %)	0.03	0.80 (85 %)	0.49	1.13 (11 %)
Rest of World	2.70 (36 %)	1.70	9.53 (68 %)	28.81	6.77 (37 %)
Total	4.55 (34 %)	2.64	16.03 (67 %)	44.64	21.61 (19 %)

[a] Primary organic aerosol is estimated using an OA/OC ratio of 1.7
[b] Fuel combustion includes fossil fuel and biofuel. Figures in brackets refer to the fraction of biofuel contribution
[c] Biomass burning emissions without biofuel contribution
[d] Secondary organic aerosols. Figures in brackets refer to the contribution of SOA oxidized from aromatics
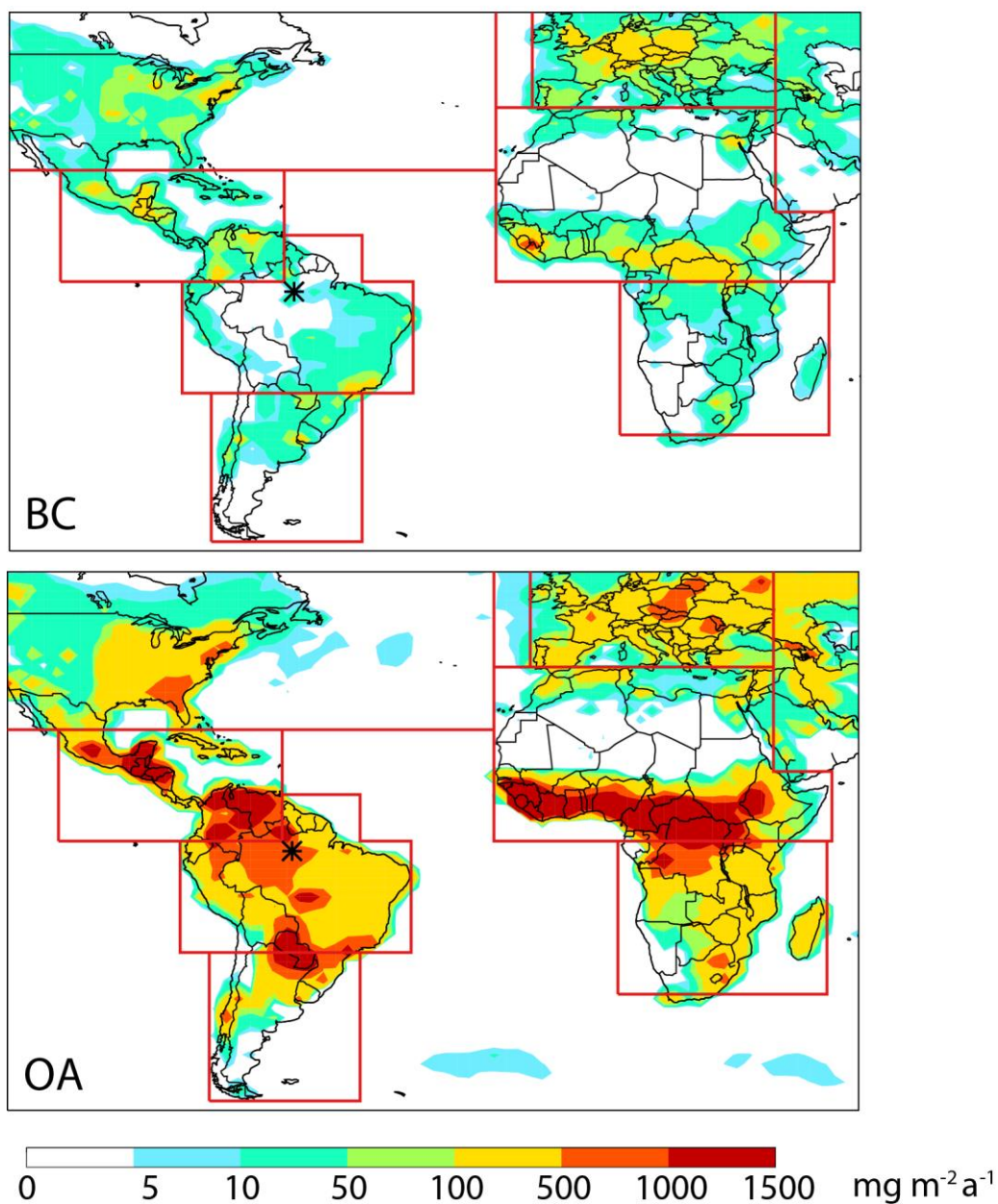
Figure 1: GEOS-Chem emissions of black carbon (BC) and organic aerosol (OA) during Jan-Apr 2014 over 120 °W–60 °E and 60 °S–60 °N. Red lines show the limits of the seven selected regions as defined in Table 2. The black asterisk is the location of ATTO.
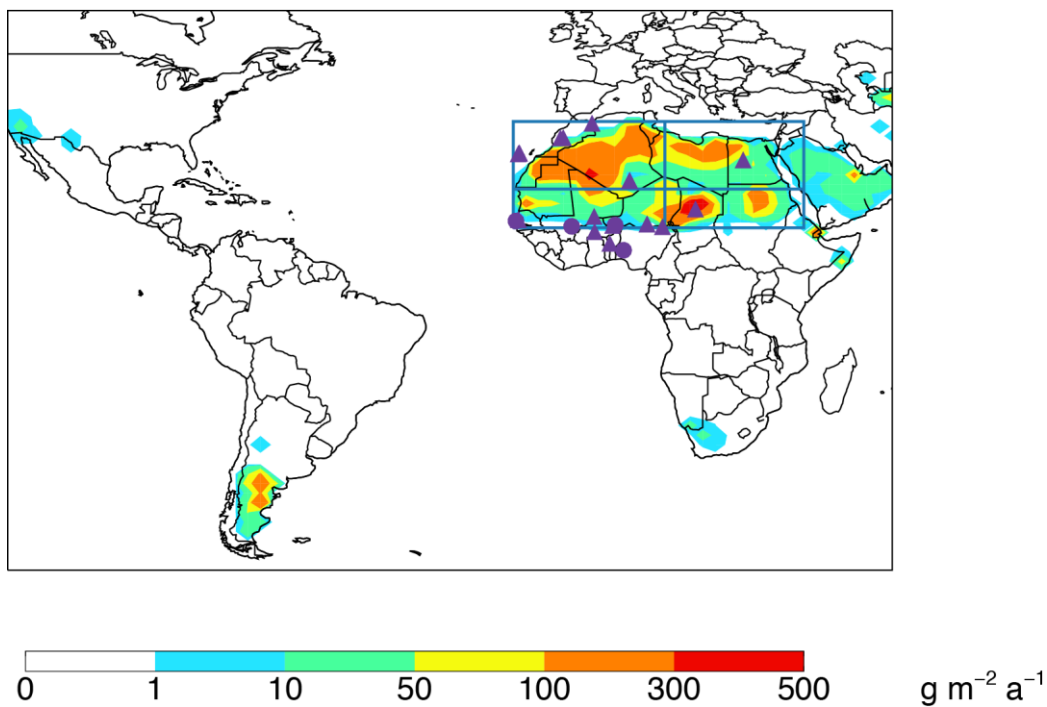
Figure 2: GEOS-Chem emissions of dust during Jan-Apr 2014 over 120 °W–60 °E and 60 °S–60 °N. Blue lines show the limits of the four selected regions for the dust sensitivity runs (see text). The purple dots and triangles are the AERONET sites used in the text.
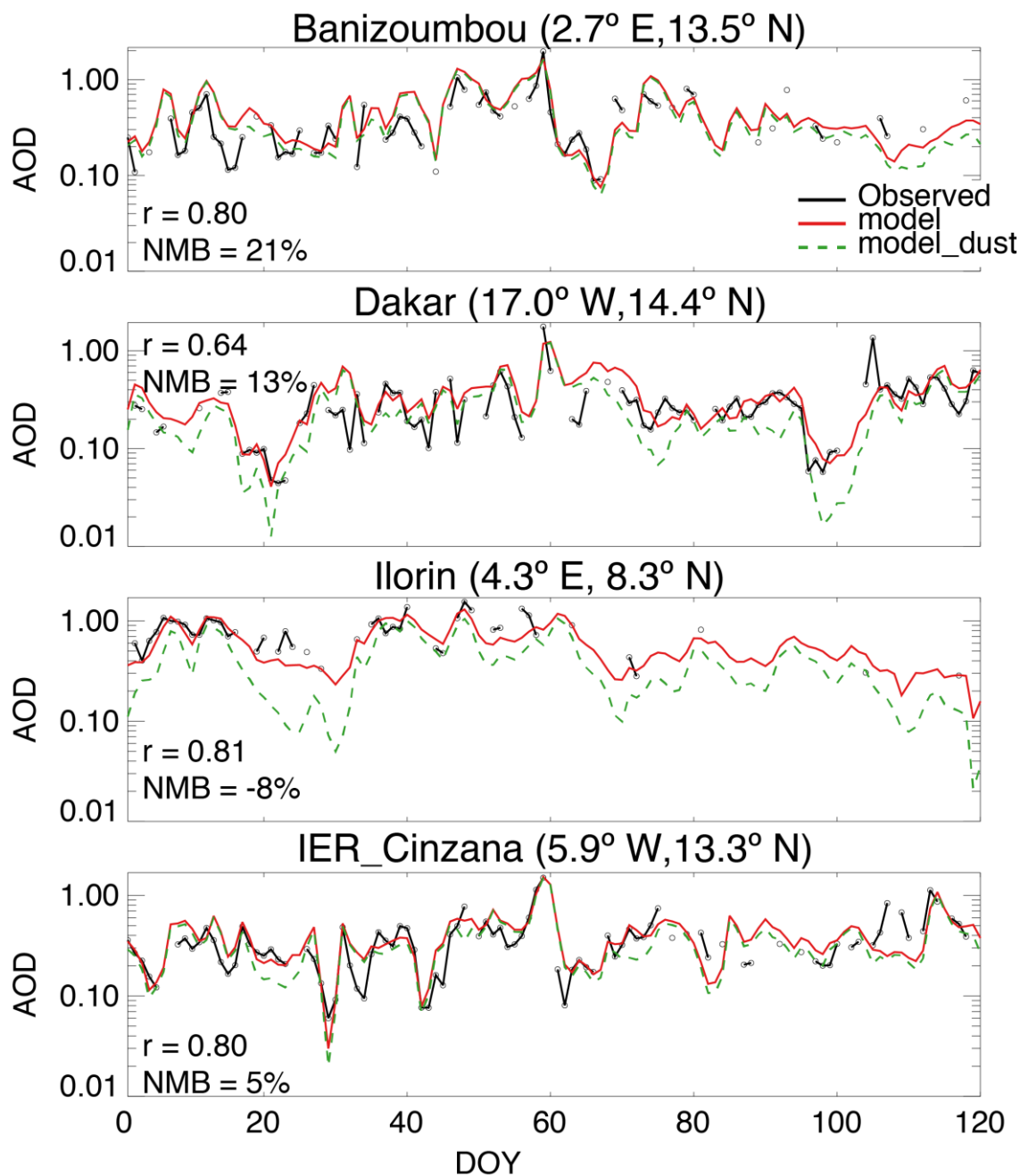
Figure 3: Time series of observed (black line) and simulated (red line) AOD at 550 nm during Jan-Apr 2014. Observations are from AERONET level 2 daily data. Model results of dust AOD are also shown as green dashed lines. Normalized mean bias (NMB) and correlation (r) statistics are shown as inset.
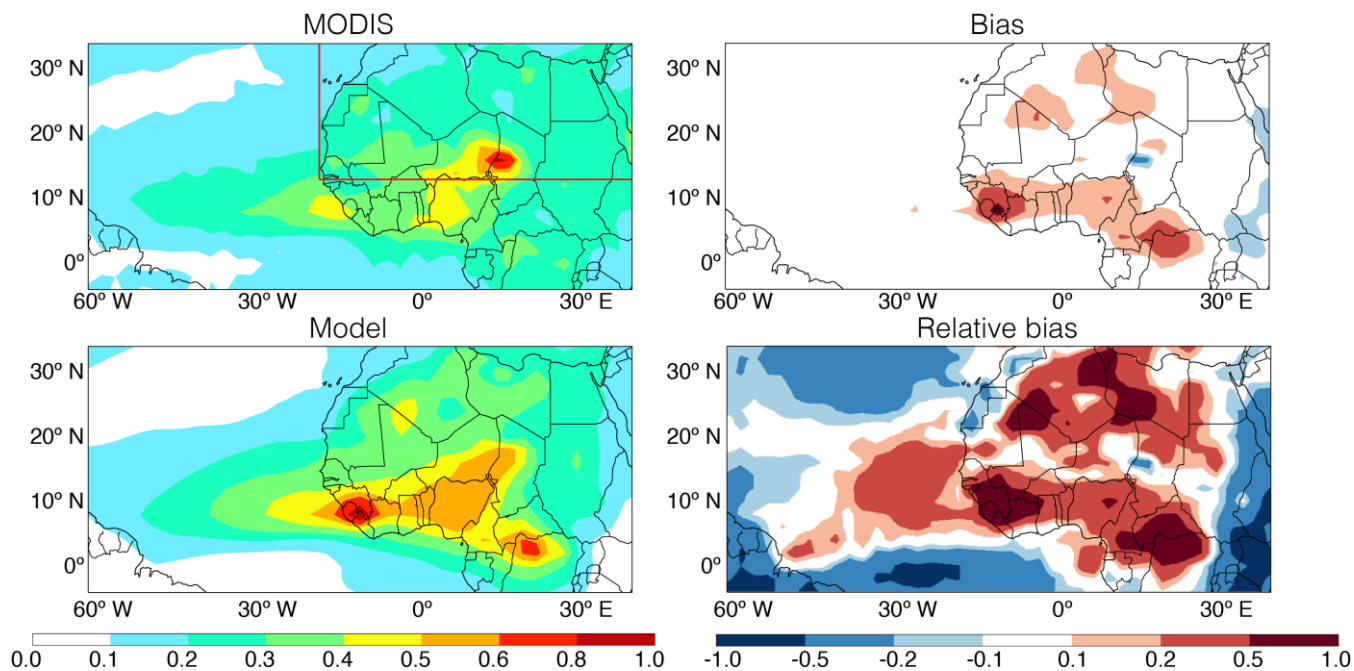
Figure 4: Spatial distributions of observed and simulated AOD at 550 nm over the rectangle region between 60 °W–40 °E and 5 ° S–35 °N averaged over Jan-Apr 2014. Observations are from MODIS level 3 daily data. The left panels are for MODIS and model AOD using the color bar at left and the right panels are for the bias (Model-MODIS) and relative bias (Model/MODIS-1) using the color bar at right. The red box in the upper left panel indicates the dusty regions defined in the text.
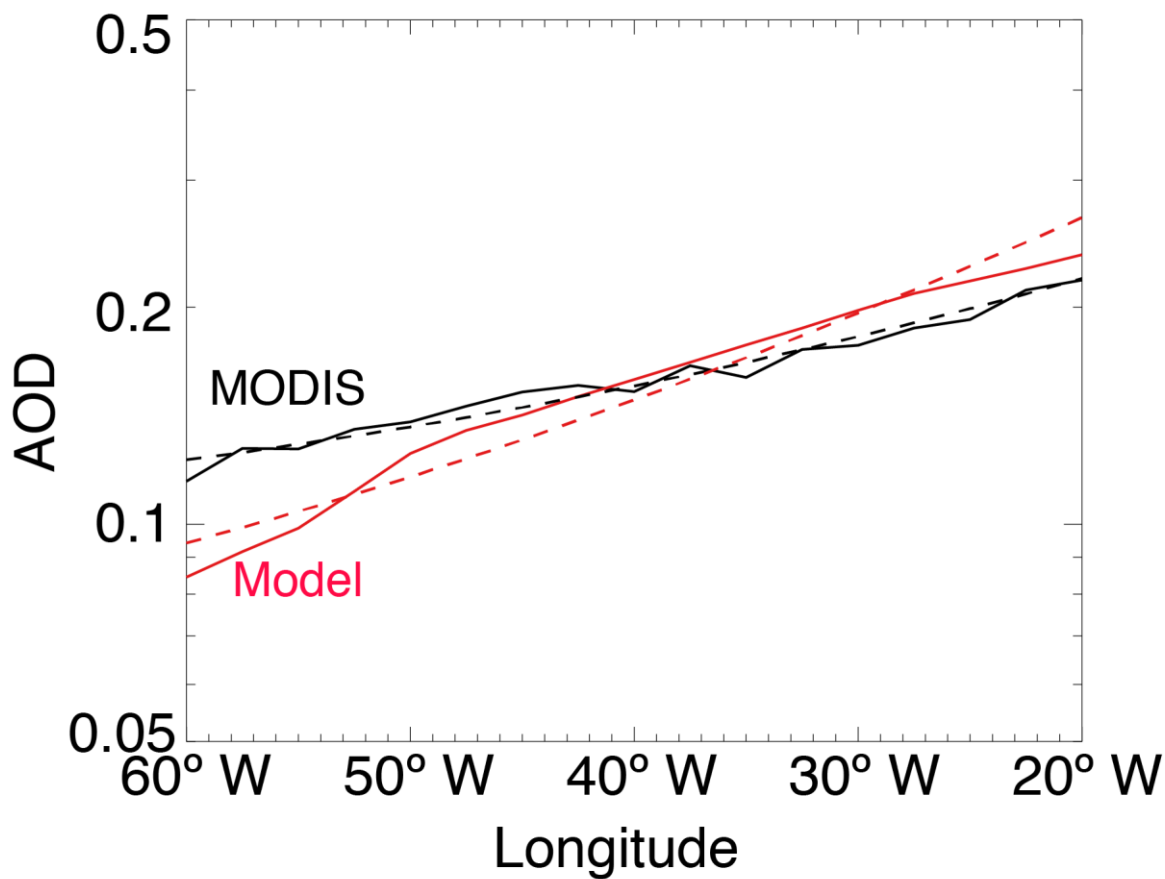
Figure 5: Seasonal AOD along transects from 20 °W to 60 °W from MODIS and model, averaged over 5 °S–25 °N and Jan-Apr 2014. The solid lines are averaged AOD and the dashed lines are the logarithmic trend line.
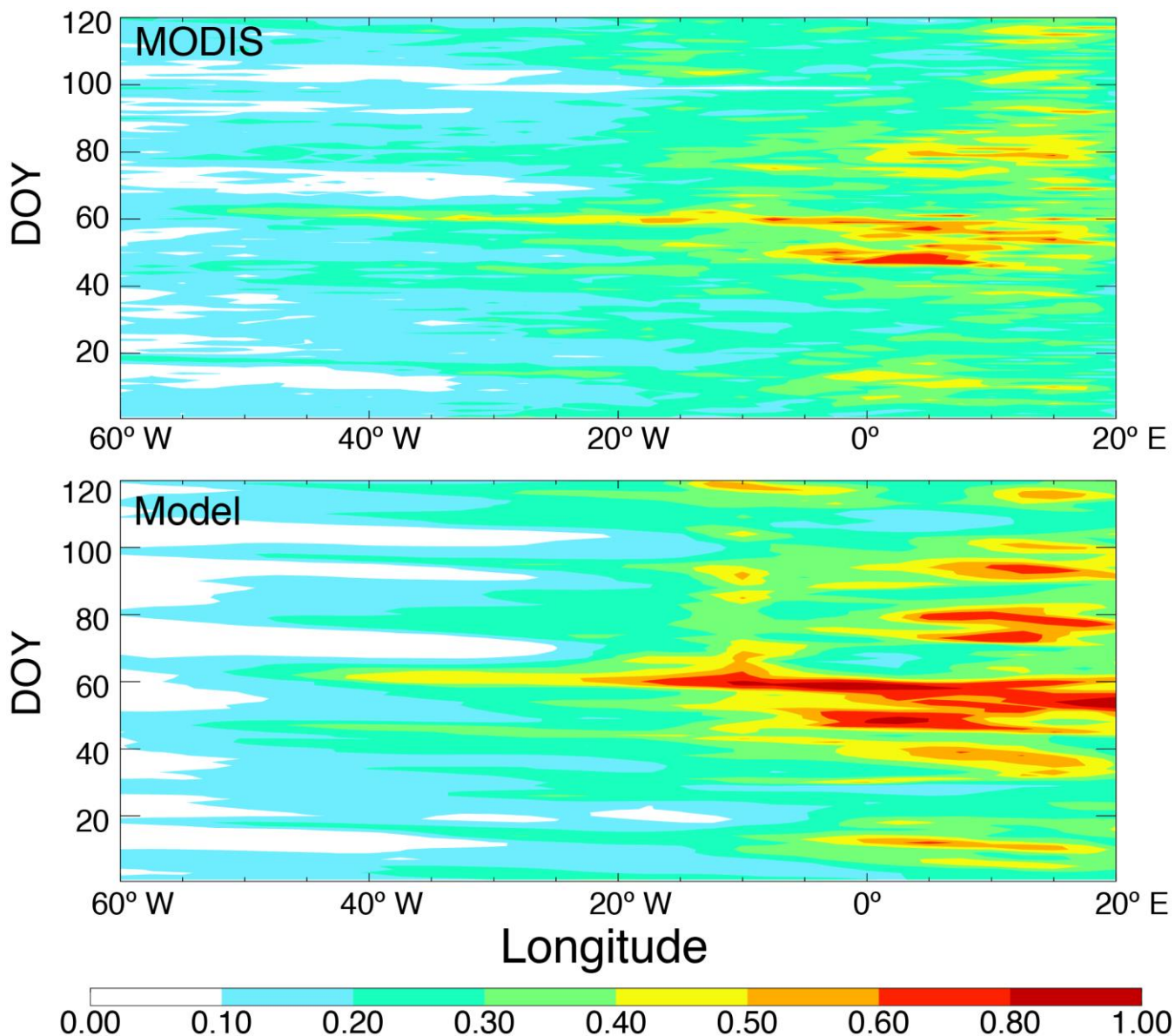
Figure 6: Daily distribution of latitudinally averaged AOD from MODIS and model over the rectangle region between 60 °W–20 ° E and 5 °S–25 °N from Jan-Apr 2014. The Y-axis is the day of year (DOY), starting with day 1 on 1 January 2014.
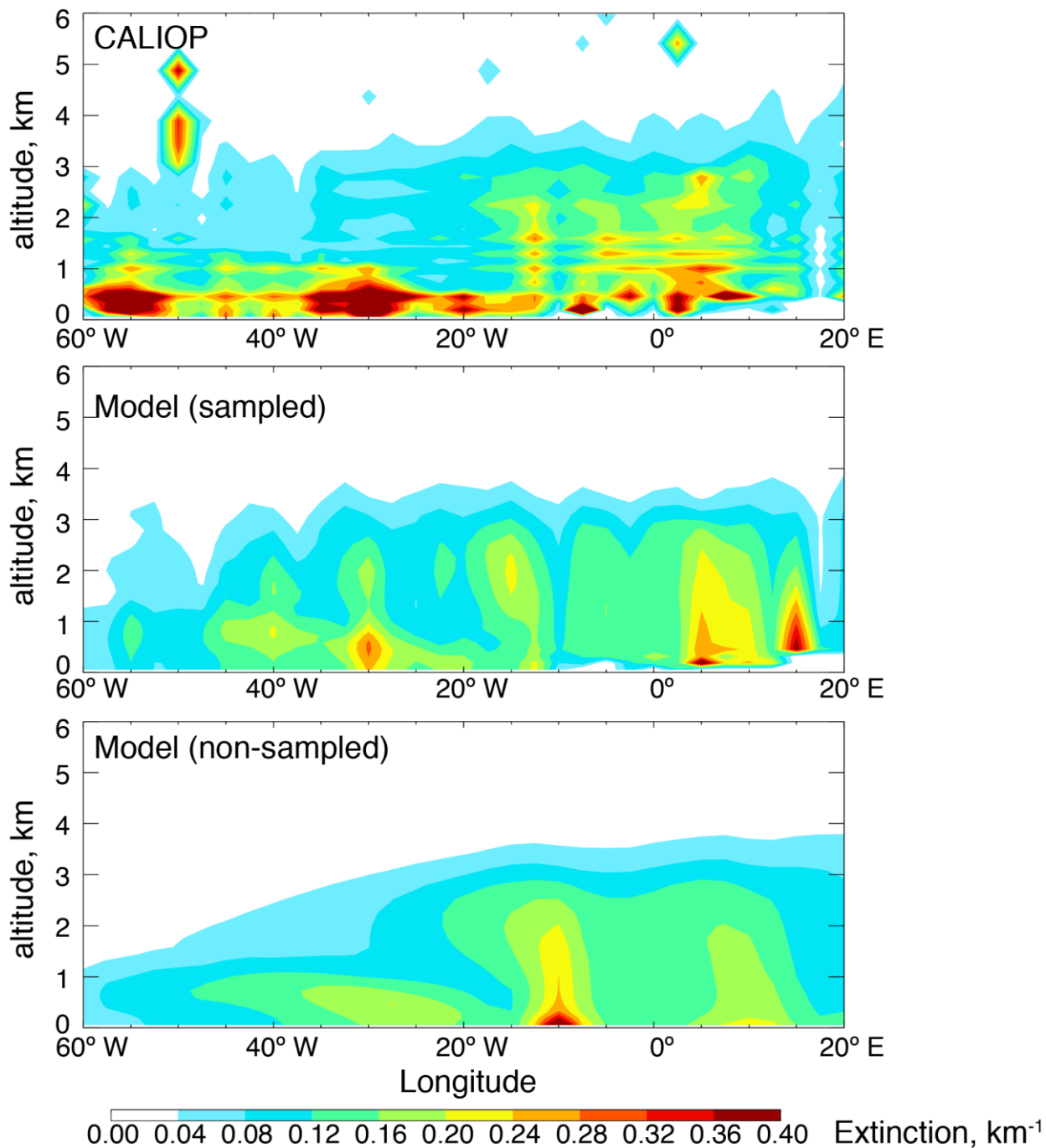
Figure 7: Curtain plots of extinction from CALIOP and model (sampled and non-sampled) averaged over 5 °–10 ° N and Jan-Apr 2014.
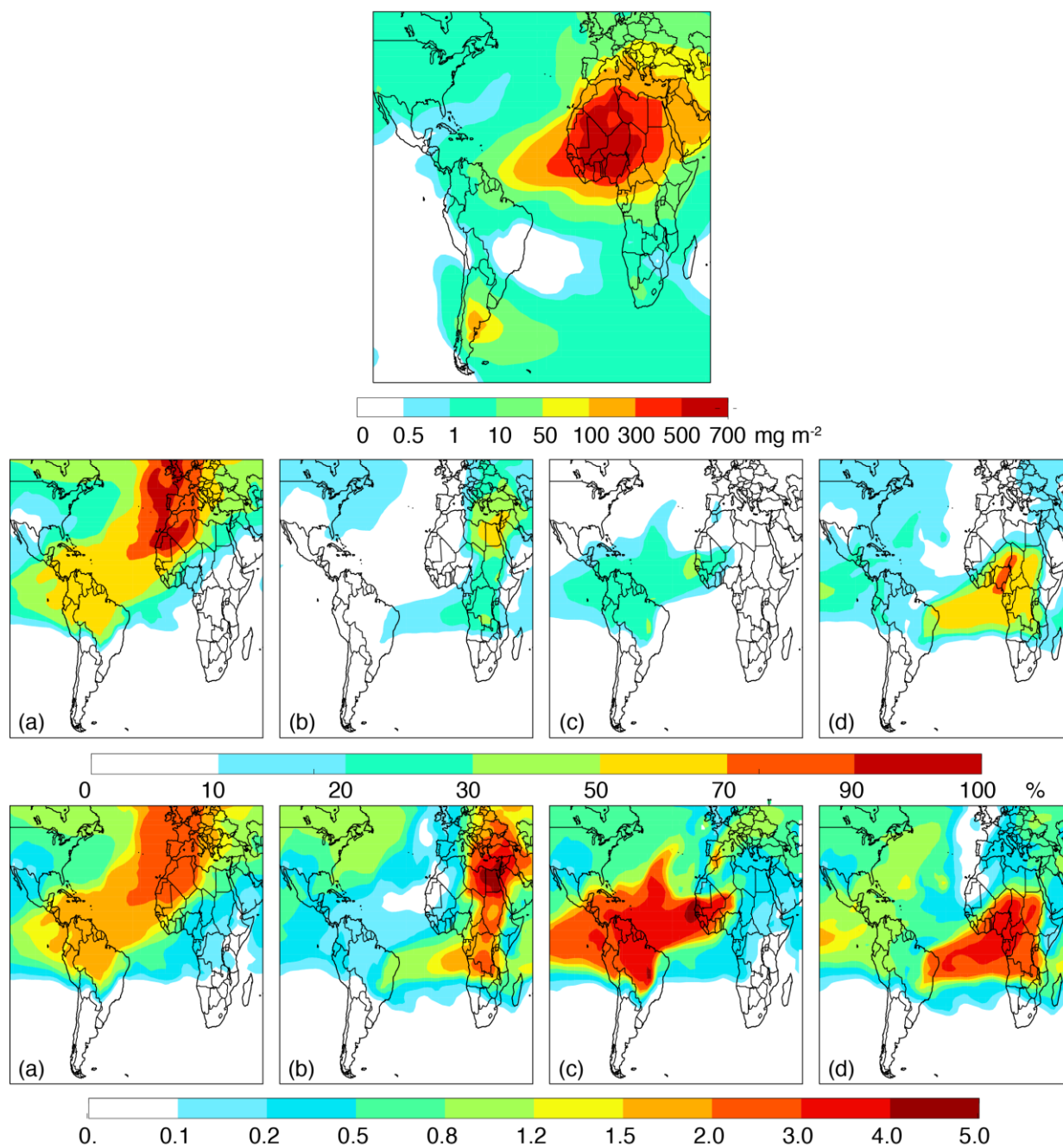
Figure 8: Column burden of total dust (top panel) and the contribution (middle panels) to total dust burden from four defined source regions (a: northwest Sahara; b: northeast Sahara; c: West Sahel; d: Bodélé) over the rectangle region between 120 °W–60 ° E and 60 °S–60 °N from Jan-Apr 2014. The bottom panels are sensitivity of dust burden to the emission from four source regions with high value indicating high sensitivity (see text).
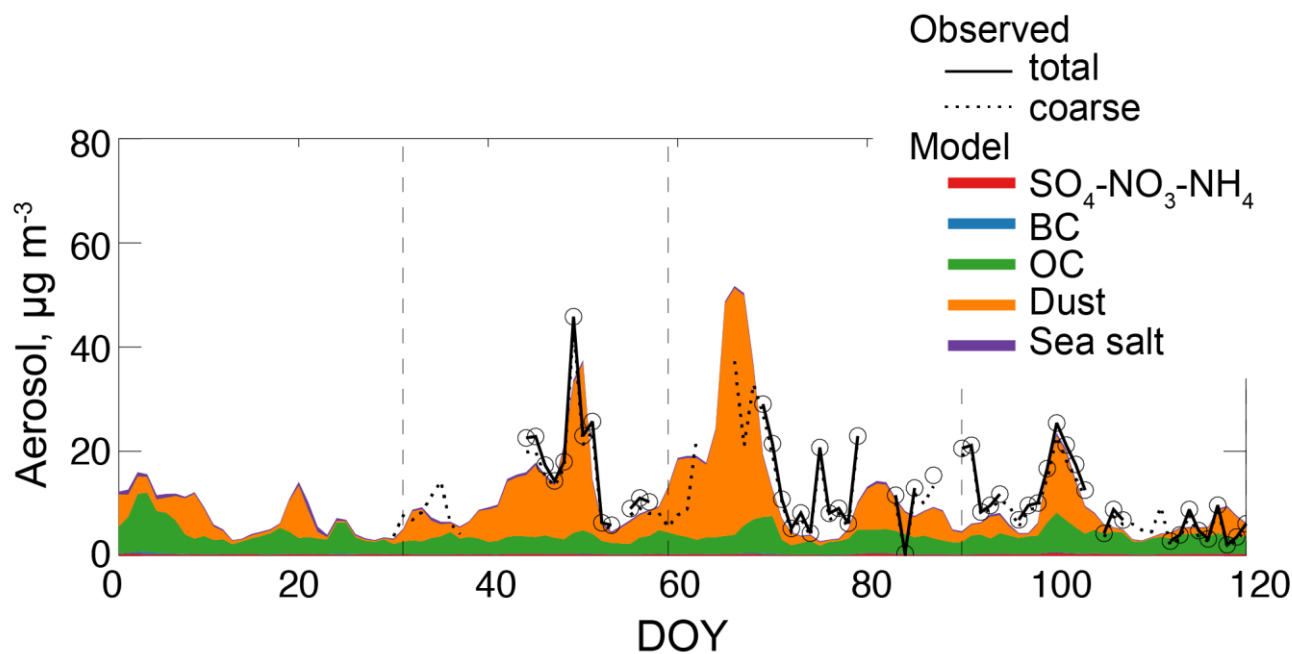
Figure 9: Time series of observed and simulated aerosol concentrations at ATTO during Jan-Apr 2014. Observed total aerosol concentrations are the sum of coarse aerosol (dp > 1µm) from OPS and fine aerosol (dp ≤ 1µm) from SMPS. Model results are separated into different species. Vertical dashed lines indicate the end of each month.
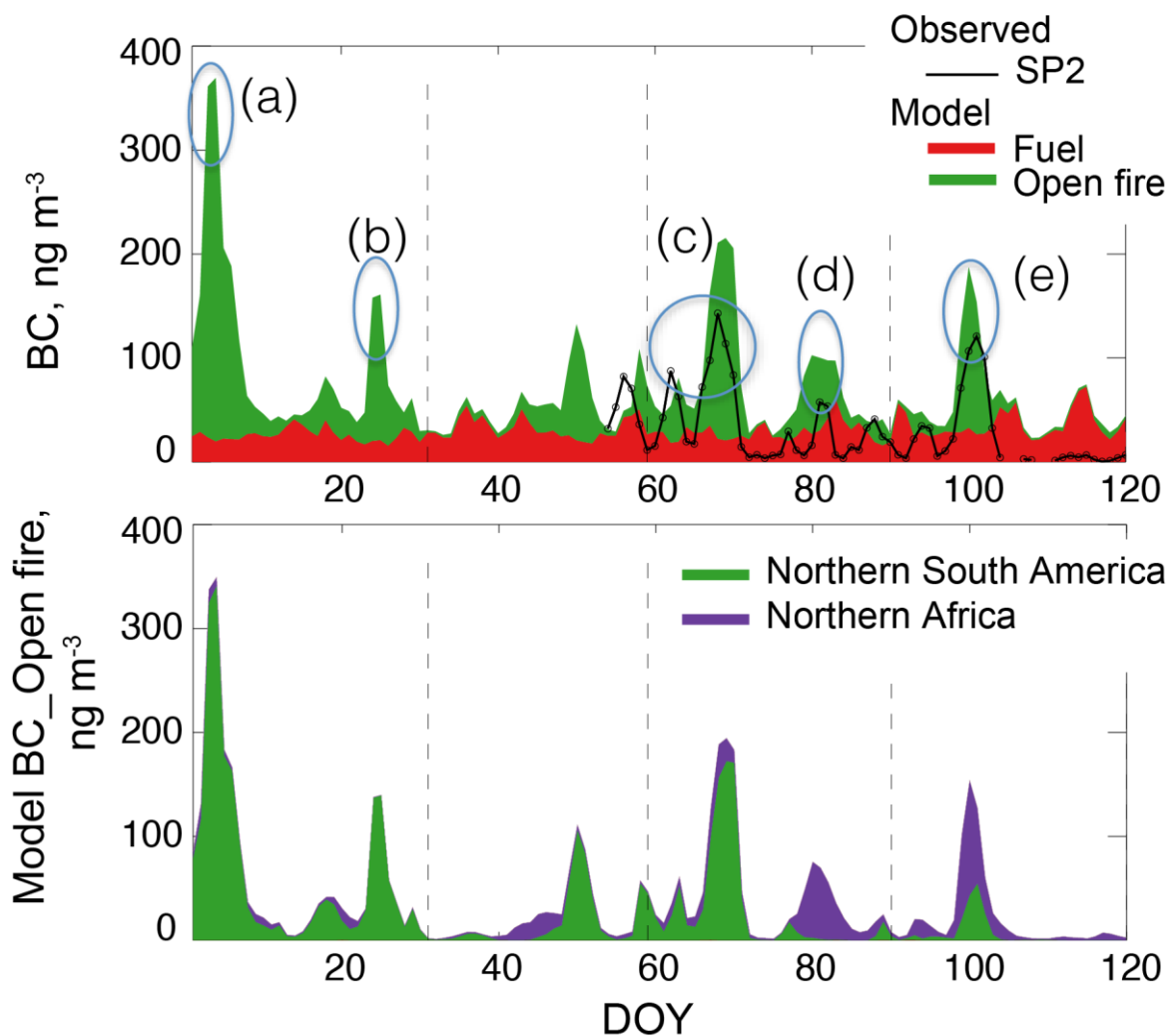
Figure 10: Time series of rBC and model BC concentrations at ATTO in Jan-Apr 2014. The top panel compares rBC with model BC separated into fuel (fossil fuel and biofuel) and open fire sources. The bottom panel further separates model fire BC by source regions. Circled peaks (a-e) are used for BC-CO analysis in Fig. 12.
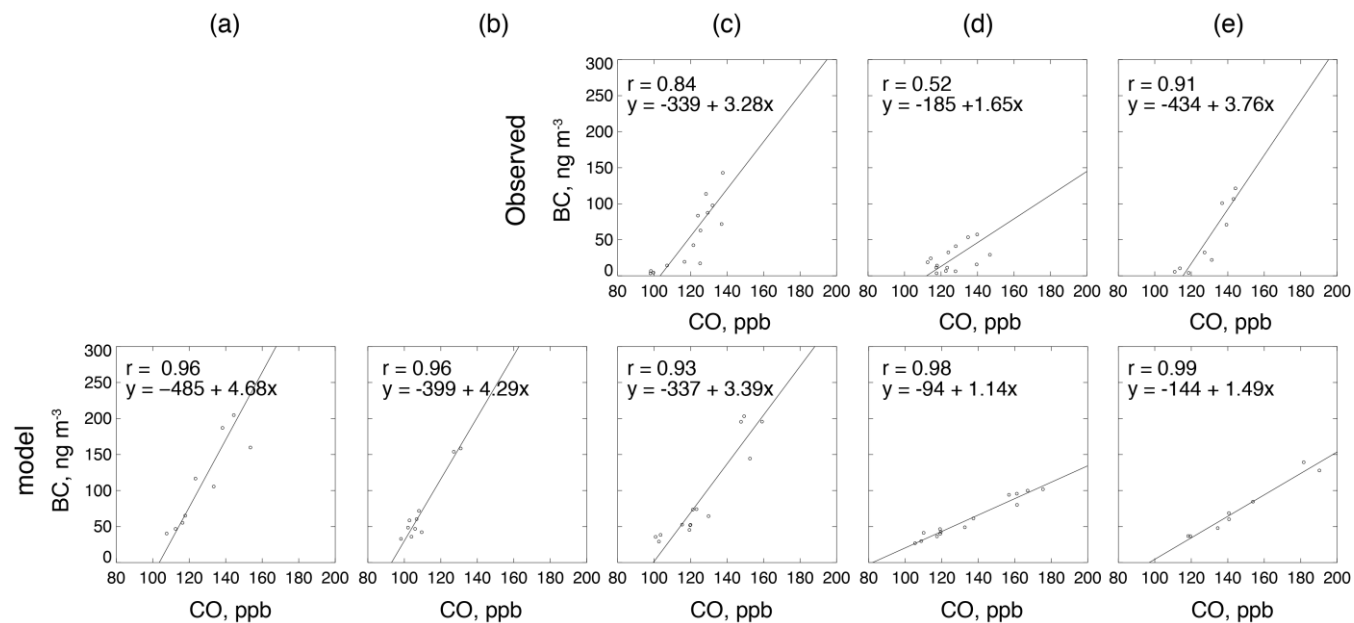
Figure 11: Scatterplots of observed (top) and simulated (bottom) BC vs. CO concentrations at ATTO for (a)-(e) peaks in Fig. 10. Reduced-major-axis (RMA) regression statistics and linear fits are shown as inset.
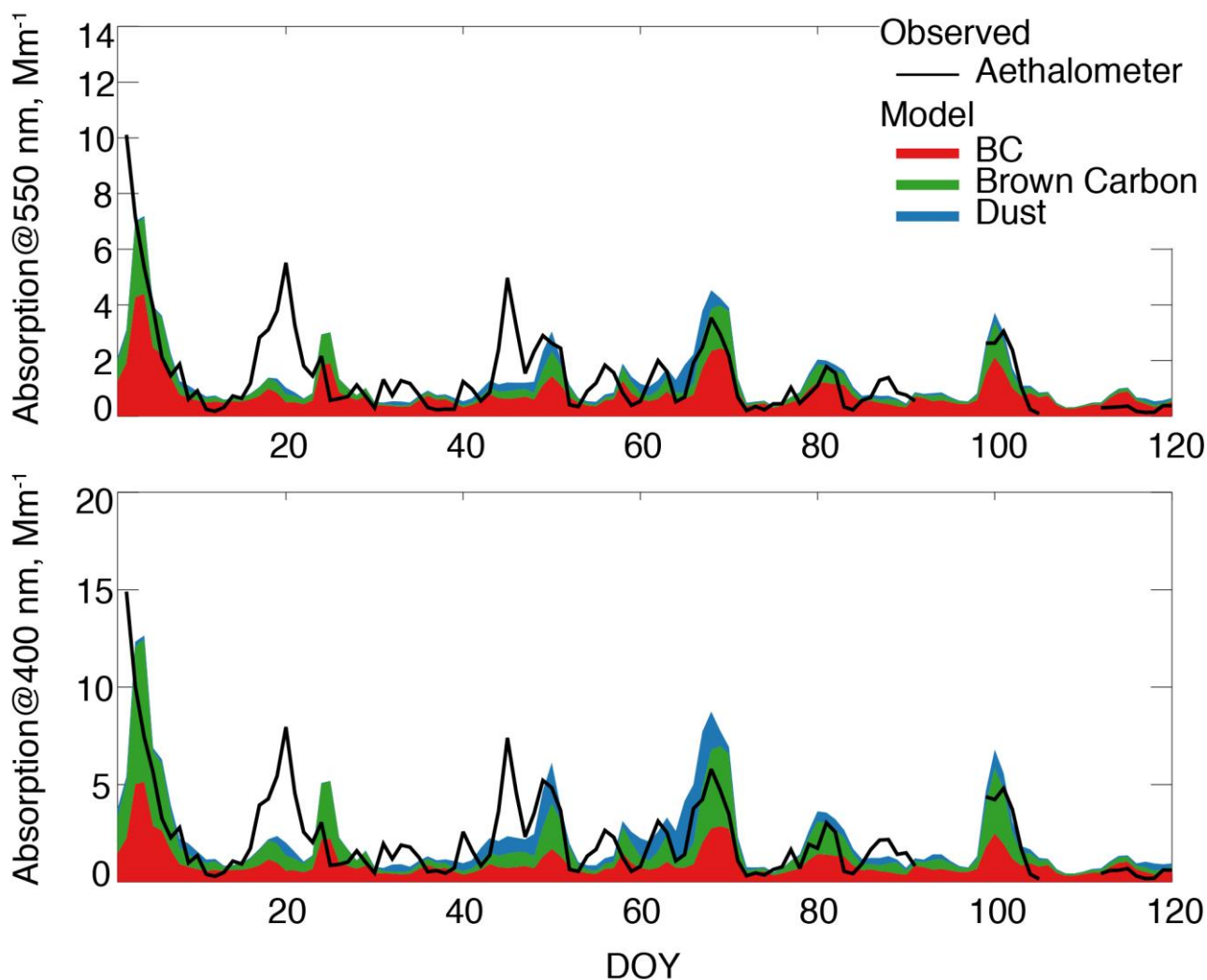
Figure 12: Time series of Aethalometer and model absorption at 550 nm (top) and 400 nm (bottom) at ATTO during Jan-Apr 2014. Model results are further separated into BC, brown carbon, and dust.
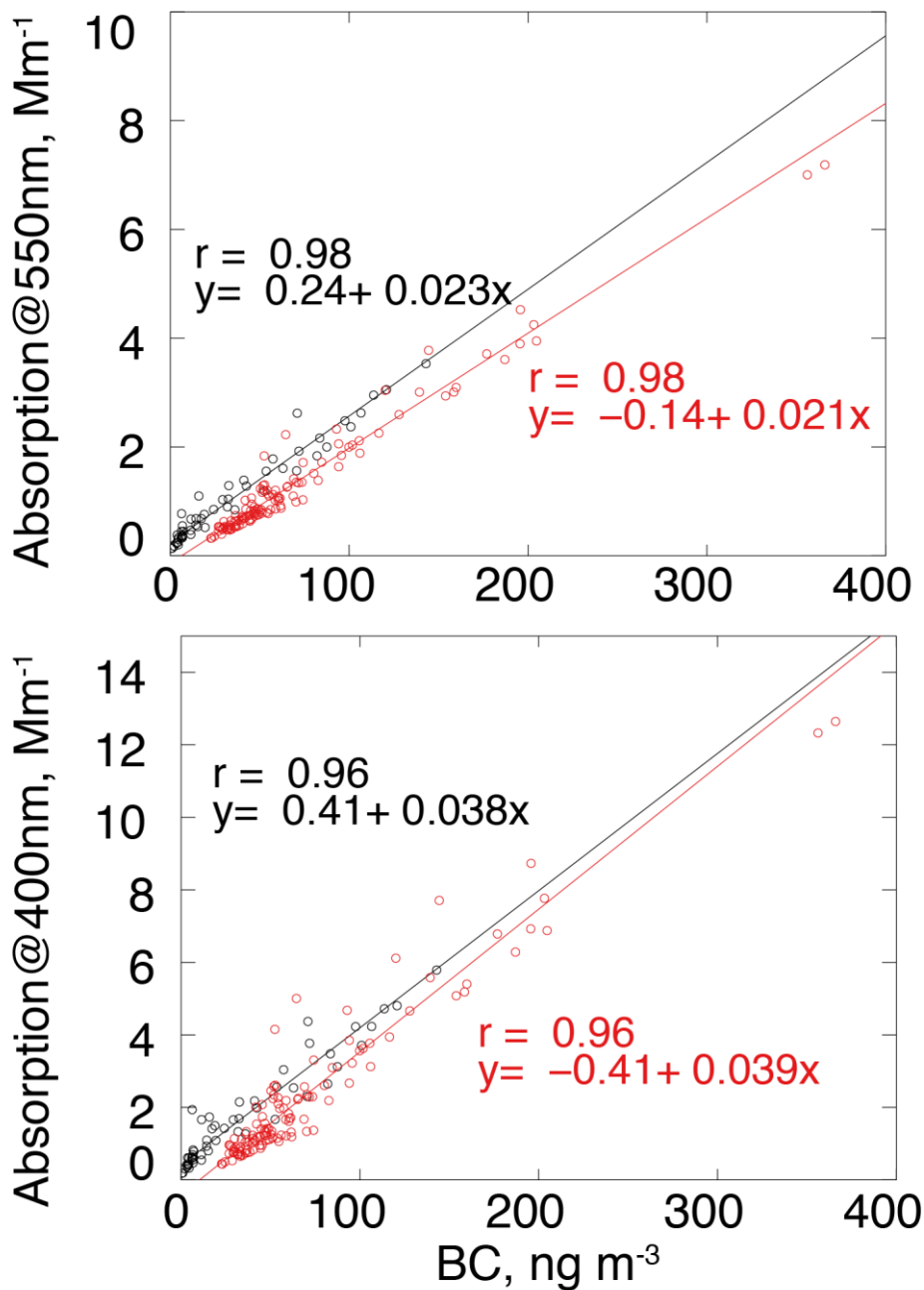
Figure 13: Scatterplot of observed (black) and simulated (red) absorption at 550 nm (top) and 400 nm (bottom) vs. BC concentrations from at ATTO in Jan-Apr 2014. Correlation coefficients and slopes of reduced-major-axis (RMA) regressions are shown as inset.
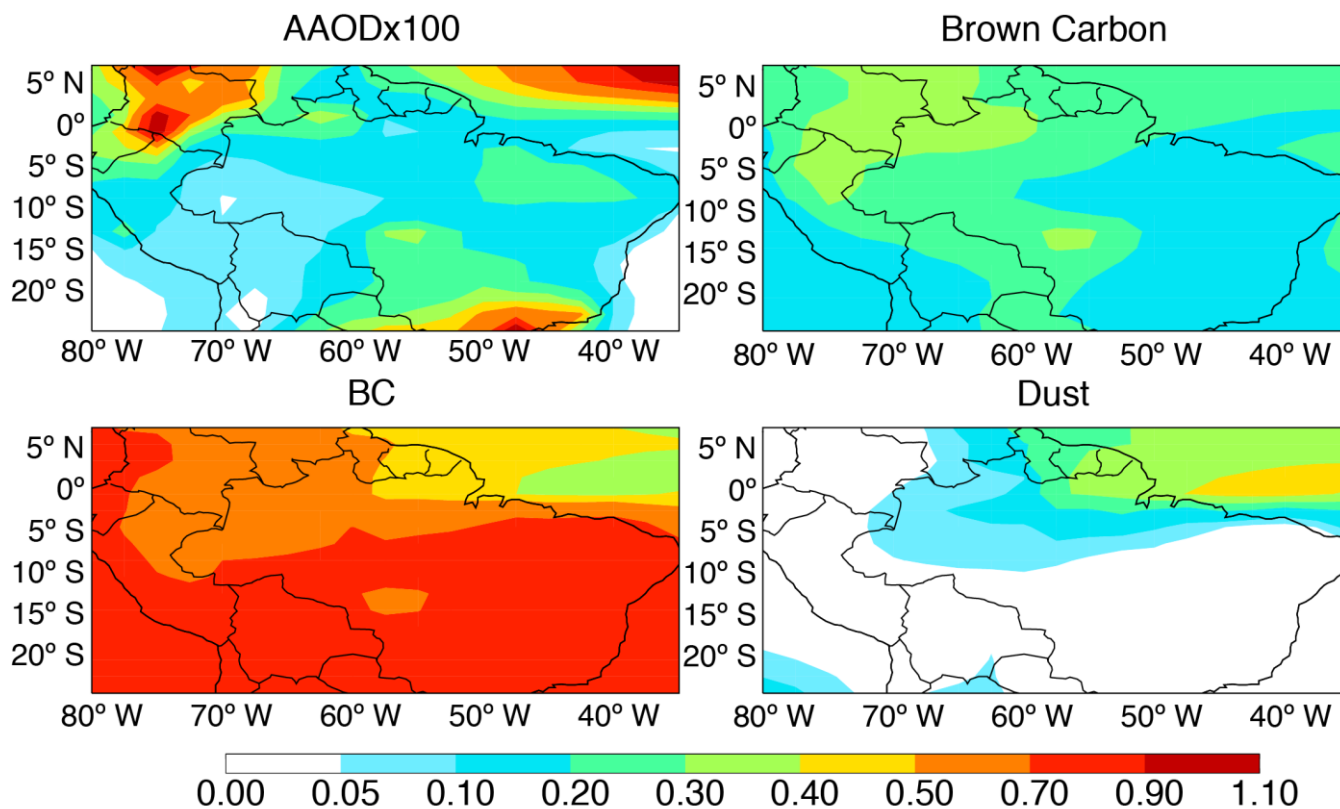
Figure 14: Model AAOD at 500 nm (left top) and the contribution to total AAOD from different components over the Amazon basin averaged over Jan-Apr 2014.
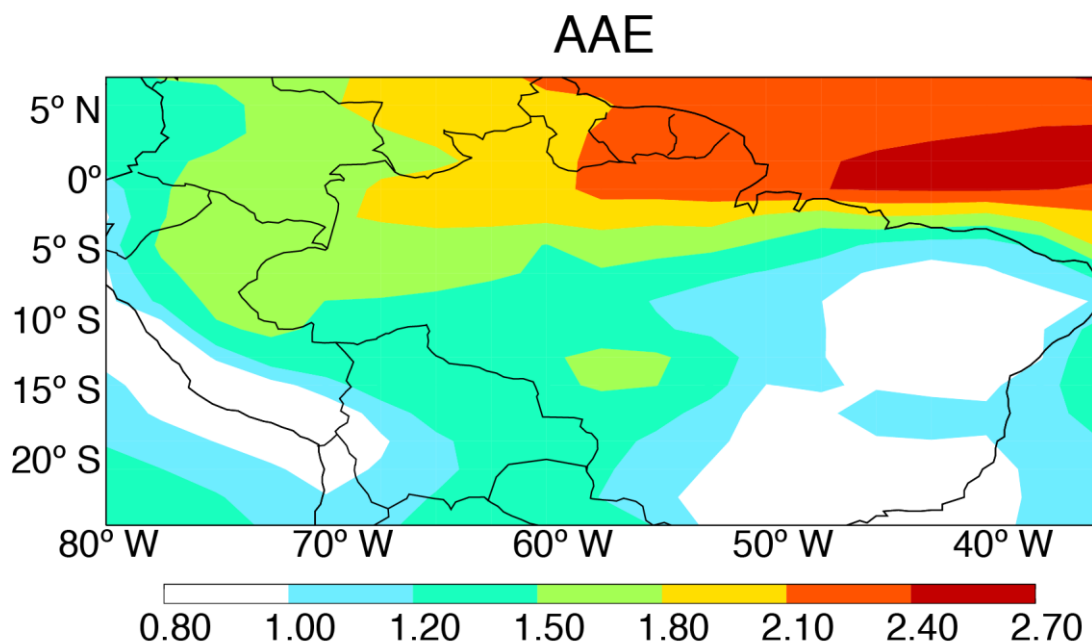
Figure 15: Model Absorption Ångström exponent (AAE) over the Amazon basin averaged over Jan-Apr 2014.